Chapter 4

Distribution Function Theories

In this chapter we describe some of the more important theoretical methods available for calculation of the pair distribution function of a uniform fluid. If the pair distribution function is known, thermodynamic properties of the system can be obtained by a number of different routes. We begin, however, by describing the way in which the distribution function is measured in radiation scattering experiments.

4.1 THE STATIC STRUCTURE FACTOR

The structure factor of a uniform fluid was defined in Section 3.6 in terms of the Fourier transform of the pair correlation function, $h(r)$. It can be defined more generally as

$$S(\mathbf{k}) = \left\langle \frac{1}{N} \rho_{\mathbf{k}} \rho_{-\mathbf{k}} \right\rangle \tag{4.1.1}$$

where $\rho_{\mathbf{k}}$ is a Fourier component of the microscopic density (3.1.2):

$$\rho_{\mathbf{k}} = \int \rho(\mathbf{r}) \exp(-i\mathbf{k} \cdot \mathbf{r}) \, d\mathbf{r} = \sum_{i=1}^{N} \exp(-i\mathbf{k} \cdot \mathbf{r}_i) \tag{4.1.2}$$

Given the δ-function representation of the pair density in (2.5.13), the definition (4.1.1) implies that in the homogeneous case:

$$\begin{aligned} S(\mathbf{k}) &= \left\langle \frac{1}{N} \sum_{i=1}^{N} \sum_{j=1}^{N} \exp(-i\mathbf{k} \cdot \mathbf{r}_i) \exp(i\mathbf{k}.\mathbf{r}_j) \right\rangle \\ &= 1 + \left\langle \frac{1}{N} \sum_{i=1}^{N} \sum_{j \neq i}^{N} \exp[-i\mathbf{k} \cdot (\mathbf{r}_i - \mathbf{r}_j)] \right\rangle \\ &= 1 + \left\langle \frac{1}{N} \sum_{i=1}^{N} \sum_{j \neq i}^{N} \iint \exp[-i\mathbf{k} \cdot (\mathbf{r} - \mathbf{r}')] \delta(\mathbf{r} - \mathbf{r}_i) \delta(\mathbf{r}' - \mathbf{r}_j) \, d\mathbf{r} \, d\mathbf{r}' \right\rangle \\ &= 1 + \frac{1}{N} \iint \exp[-i\mathbf{k} \cdot (\mathbf{r} - \mathbf{r}')] \rho_N^{(2)}(\mathbf{r} - \mathbf{r}') \, d\mathbf{r} \, d\mathbf{r}' \\ &= 1 + \rho \int g(r) \exp(-i\mathbf{k} \cdot \mathbf{r}) \, d\mathbf{r} \end{aligned} \tag{4.1.3}$$

Theory of Simple Liquids, Fourth Edition. http://dx.doi.org/10.1016/B978-0-12-387032-2.00004-0

In the last step we have used the definition (2.5.8) of the pair distribution function and exploited the fact that the system is translationally invariant in order to integrate over $\mathbf{r}'$. Conversely, $g(r)$ is given by the inverse transform

$$\rho g(\mathbf{r}) = (2\pi)^{-3} \int [S(\mathbf{k}) - 1] \exp(i\mathbf{k} \cdot \mathbf{r})\, \mathrm{d}\mathbf{k} \tag{4.1.4}$$

The final result in (4.1.3) can also be written as

$$S(\mathbf{k}) = 1 + (2\pi)^3 \rho \delta(\mathbf{k}) + \rho \hat{h}(\mathbf{k}) \tag{4.1.5}$$

The definitions (3.6.10) and (4.1.1) are therefore equivalent apart from a δ-function term, which henceforth we shall ignore. Experimentally (see below) that term corresponds to radiation which passes through the sample unscattered.

The structure factor of a fluid can be determined experimentally from measurements of the cross-section for scattering of neutrons or X-rays by the fluid as a function of scattering angle. Here we give a simplified treatment of the calculation of the neutron cross-section in terms of $S(\mathbf{k})$.

Let us suppose that an incident neutron is scattered by the sample through an angle θ. The incoming neutron can be represented as a plane wave:

$$\psi_1(\mathbf{r}) = \exp(i\mathbf{k}_1 \cdot \mathbf{r}) \tag{4.1.6}$$

while at sufficiently large distances from the sample the scattered neutron can be represented as a spherical wave:

$$\psi_2(\mathbf{r}) \sim \frac{\exp(ik_2 r)}{r} \tag{4.1.7}$$

Thus, asymptotically ($r \to \infty$), the wave function of the neutron behaves as

$$\psi(\mathbf{r}) \sim \exp(i\mathbf{k}_1 \cdot \mathbf{r}) + f(\theta) \frac{\exp(ik_2 r)}{r} \tag{4.1.8}$$

and the amplitude $f(\theta)$ of the scattered component is related to the differential cross-section $\mathrm{d}\sigma/\mathrm{d}\Omega$ for scattering into a solid angle $\mathrm{d}\Omega$ in the direction θ, ϕ by

$$\frac{\mathrm{d}\sigma}{\mathrm{d}\Omega} = |f(\theta)|^2 \tag{4.1.9}$$

The geometry of a scattering event is illustrated in Figure 4.1. The momentum transferred from neutron to sample in units of $\hbar$ is

$$\mathbf{k} = \mathbf{k}_1 - \mathbf{k}_2 \tag{4.1.10}$$

To simplify the calculation we assume that the scattering is elastic. Then $|\mathbf{k}_1| = |\mathbf{k}_2|$ and

$$k = 2k_1 \sin\frac{1}{2}\theta = \frac{4\pi}{\lambda} \sin\frac{1}{2}\theta \tag{4.1.11}$$

where λ is the neutron wavelength.

The scattering of the neutron occurs as the result of interactions with the atomic nuclei. These interactions are very short ranged, and the total

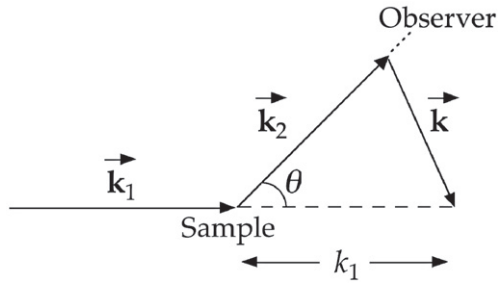

FIGURE 4.1 Geometry of an elastic scattering event.

scattering potential $\mathcal{V}(\mathbf{r})$ may therefore be approximated by a sum of δ-function pseudopotentials in the form

$$\mathcal{V}(\mathbf{r}) = \frac{2\pi\hbar^2}{m}\sum_{i=1}^{N} b_i\delta(\mathbf{r}-\mathbf{r}_i) \tag{4.1.12}$$

where b_i is the *scattering length* of the ith nucleus and m is the neutron mass. For most nuclei, b_i is positive, but it may also be negative and even complex; it varies both with isotopic species and with the spin state of the nucleus.

The wave function $\psi(\mathbf{r})$ must be a solution of the Schrödinger equation:

$$\left(-\frac{\hbar^2}{2m}\nabla^2 + \mathcal{V}(\mathbf{r})\right)\psi(\mathbf{r}) = E\psi(\mathbf{r}) \tag{4.1.13}$$

The general solution having the correct asymptotic behaviour is

$$\psi(\mathbf{r}) = \exp(i\mathbf{k}_1\cdot\mathbf{r}) - \frac{m}{2\pi\hbar^2}\int \frac{\exp(ik_1|\mathbf{r}-\mathbf{r}'|)}{|\mathbf{r}-\mathbf{r}'|}\mathcal{V}(\mathbf{r}')\psi(\mathbf{r}')\,\mathrm{d}\mathbf{r}' \tag{4.1.14}$$

where the second term on the right-hand side represents a superposition of spherical waves emanating from each point in the sample.

Equation (4.1.14) is an integral equation for $\psi(\mathbf{r})$. The solution in the case when the interaction $\mathcal{V}(\mathbf{r})$ is weak is obtained by setting $\psi(\mathbf{r}) \approx \exp(i\mathbf{k}_1\cdot\mathbf{r})$ inside the integral sign. This substitution yields the so-called first Born approximation to $\psi(\mathbf{r})$:

$$\psi(\mathbf{r}) \approx \exp(i\mathbf{k}_1\cdot\mathbf{r}) - \frac{m}{2\pi\hbar^2}\int \frac{\exp(ik_1|\mathbf{r}-\mathbf{r}'|)}{|\mathbf{r}-\mathbf{r}'|}\mathcal{V}(\mathbf{r}')\exp(i\mathbf{k}_1\cdot\mathbf{r}')\,\mathrm{d}\mathbf{r}' \tag{4.1.15}$$

from which an expression for $f(\theta)$ is obtained by taking the $r\to\infty$ limit and matching the result to the known, asymptotic form of $\psi(\mathbf{r})$ given by (4.1.8). If $|\mathbf{r}| \gg |\mathbf{r}'|$, then

$$|\mathbf{r}-\mathbf{r}'| = (r^2 + r'^2 - 2\mathbf{r}\cdot\mathbf{r}')^{1/2} \approx r - \hat{\mathbf{r}}\cdot\mathbf{r}' \tag{4.1.16}$$

where $\hat{\mathbf{r}}$ is a unit vector in the direction of $\mathbf{r}$. Since we have assumed that the scattering is elastic, $k_1\hat{\mathbf{r}} = \mathbf{k}_2$. Thus, as $r \to \infty$:

$$\psi(\mathbf{r}) \sim \exp(i\mathbf{k}_1 \cdot \mathbf{r}) - \frac{\exp(ik_1 r)}{r} \frac{m}{2\pi\hbar^2} \int \exp(-i\mathbf{k}_2 \cdot \mathbf{r}')\mathcal{V}(\mathbf{r}') \times \exp(i\mathbf{k}_1 \cdot \mathbf{r}')\, \mathrm{d}\mathbf{r}' \tag{4.1.17}$$

By comparing (4.1.17) with (4.1.8), and remembering that $k_1 = k_2$, we find that

$$\begin{aligned} f(\theta) &= -\frac{m}{2\pi\hbar^2} \int \exp(-i\mathbf{k}_2 \cdot \mathbf{r})\mathcal{V}(\mathbf{r}) \exp(i\mathbf{k}_1 \cdot \mathbf{r})\, \mathrm{d}\mathbf{r} \\ &= -\frac{m}{2\pi\hbar^2} \int \mathcal{V}(\mathbf{r}) \exp(i\mathbf{k} \cdot \mathbf{r})\, \mathrm{d}\mathbf{r} \end{aligned} \tag{4.1.18}$$

Hence the amplitude of the scattered component is proportional to the Fourier transform of the scattering potential. The first line of (4.1.18) also shows that $f(\theta)$ is expressible as a matrix element of the interaction $\mathcal{V}(\mathbf{r})$ between initial and final plane-wave states of the neutron. Use of the first Born approximation is therefore equivalent to calculating the cross-section $\mathrm{d}\sigma/\mathrm{d}\Omega$ by the 'golden rule' of quantum mechanical perturbation theory.

An expression for $\mathrm{d}\sigma/\mathrm{d}\Omega$ can now be derived by substituting for $\mathcal{V}(\mathbf{r})$ in (4.1.18), inserting the result in (4.1.9) and taking the thermal average. This yields the expression

$$\begin{aligned} \frac{\mathrm{d}\sigma}{\mathrm{d}\Omega} &= \left\langle \left| \sum_{i=1}^{N} b_i \exp(-i\mathbf{k} \cdot \mathbf{r}_i) \right|^2 \right\rangle \\ &= \left\langle \sum_{i=1}^{N} \sum_{j=1}^{N} b_i b_j \exp[-i\mathbf{k} \cdot (\mathbf{r}_j - \mathbf{r}_i)] \right\rangle \end{aligned} \tag{4.1.19}$$

A more useful result is obtained by taking an average of the scattering lengths over isotopes and nuclear spin states, which can be done independently of the thermal averaging over coordinates. We therefore introduce the notation

$$\begin{aligned} &\left\langle b_i^2 \right\rangle \equiv \left\langle b^2 \right\rangle, \quad \left\langle b_i b_j \right\rangle = \left\langle b_i \right\rangle \left\langle b_j \right\rangle \equiv \langle b \rangle^2 \\ &\langle b \rangle^2 \equiv b_{\mathrm{coh}}^2, \quad \left(\left\langle b^2 \right\rangle - \langle b \rangle^2 \right) \equiv b_{\mathrm{inc}}^2 \end{aligned} \tag{4.1.20}$$

and rewrite (4.1.19) as

$$\begin{aligned} \frac{\mathrm{d}\sigma}{\mathrm{d}\Omega} &= N\left\langle b^2 \right\rangle + \langle b \rangle^2 \left\langle \sum_{i=1}^{N} \sum_{j \neq i}^{N} \exp[-i\mathbf{k} \cdot (\mathbf{r}_i - \mathbf{r}_j)] \right\rangle \\ &= N\left(\left\langle b^2 \right\rangle - \langle b \rangle^2 \right) + \langle b \rangle^2 \left\langle \left| \sum_{i=1}^{N} \exp(-i\mathbf{k} \cdot \mathbf{r}_i) \right|^2 \right\rangle \\ &= N b_{\mathrm{inc}}^2 + N b_{\mathrm{coh}}^2 S(\mathbf{k}) \end{aligned} \tag{4.1.21}$$

The subscripts 'coh' and 'inc' refer, respectively, to *coherent* and *incoherent* scattering. Information about the structure of the fluid is contained entirely within the coherent contribution to the cross-section; there is no incoherent contribution if the sample consists of one isotopic species of zero nuclear spin. The amplitude of the wave scattered by a single, fixed nucleus is

$$f(\theta) = -b \int \delta(\mathbf{r}) \exp(i\mathbf{k} \cdot \mathbf{r}) \, \mathrm{d}\mathbf{r} = -b \tag{4.1.22}$$

In the absence of incoherent scattering the cross-section for scattering by a liquid is

$$\frac{\mathrm{d}\sigma}{\mathrm{d}\Omega} = Nb^2 S(\mathbf{k}) \tag{4.1.23}$$

where Nb^2 is the cross-section for a system of N independent nuclei and $S(\mathbf{k})$ represents the effects of spatial correlations.

A similar calculation can be made of the cross-section for elastic scattering of X-rays. There is now no separation into coherent and incoherent parts, but the expression for the differential cross-section has the same general form as in (4.1.23). One important difference is that X-rays are scattered by interaction with the atomic electrons and the analogue of the neutron scattering length is the atomic *form factor*, $f(\mathbf{k})$. The latter, unlike b, is a function of $\mathbf{k}$ and defined as

$$f(\mathbf{k}) = \left\langle \sum_{n=1}^{Z} \exp\left[i\mathbf{k} \cdot \left(\mathbf{r}_i^{(n)} - \mathbf{r}_i \right) \right] \right\rangle_{\mathrm{Q}} \tag{4.1.24}$$

where the subscript Q denotes a quantum mechanical expectation value, $\mathbf{r}_i^{(n)}$ represents the coordinates of the nth electron of the ith atom (with nuclear coordinates $\mathbf{r}_i$) and Z is the atomic number; for large atoms, $f(\mathbf{k}) \approx Z$ over the range of $\mathbf{k}$ in which $S(\mathbf{k})$ displays a significant degree of structure.

The pair distribution function is derived from a measured structure factor, such as that pictured in Figure 3.2, by numerically transforming the experimental data according to (4.1.4). Difficulties arise in practice because measurements of $S(\mathbf{k})$ necessarily introduce a cut-off at large values of k. These difficulties are the source of the unphysical ripples seen at small r in the distribution function for liquid argon shown in Figure 2.1.

The definition of the structure factor given by (4.1.1) is easily extended to systems of more than one component. As in Section 3.6, we consider an n-component system in which the number concentration of species ν is x_ν. The microscopic partial density $\rho^\nu(\mathbf{r})$ and its Fourier components $\rho_{\mathbf{k}}^\nu$ are defined in a manner analogous to (3.1.2) and (4.1.2), except that the sums run only over the particles of species ν. Thus

$$\rho_{\mathbf{k}}^\nu = \sum_{i=1}^{N_\nu} \exp(-i\mathbf{k} \cdot \mathbf{r}_i) \tag{4.1.25}$$

If the fluid is homogeneous, the partial pair distribution function

$$g_{\nu\mu}(\mathbf{r}) = h_{\nu\mu}(\mathbf{r}) + 1 \tag{4.1.26}$$

has a δ-function representation given by

$$x_\nu x_\mu \rho g_{\nu\mu}(\mathbf{r}) = \left\langle \frac{1}{N} \sum_{i=1}^{N_\nu} \sum_{j=1}^{N_\mu} \delta(\mathbf{r} + \mathbf{r}_i - \mathbf{r}_j) \right\rangle \tag{4.1.27}$$

The partial structure factor defined by a generalisation of (4.1.1) as

$$S_{\nu\mu}(\mathbf{k}) = \left\langle \frac{1}{N} \rho_{\mathbf{k}}^{\nu} \rho_{-\mathbf{k}}^{\mu} \right\rangle \tag{4.1.28}$$

is related to $g_{\nu\mu}(r)$ by

$$S_{\nu\mu}(\mathbf{k}) = x_\nu \delta_{\nu\mu} + x_\nu x_\mu \rho \int g_{\nu\mu}(r) \exp(-i\mathbf{k} \cdot \mathbf{r})\, \mathrm{d}\mathbf{r} \tag{4.1.29}$$

which again differs from the earlier definition (3.6.15) by an unimportant δ-function term.

4.2 THE YBG HIERARCHY AND THE BORN–GREEN EQUATION

It was shown in Section 2.1 that the non-equilibrium phase-space distribution functions $f^{(n)}(\mathbf{r}^n, \mathbf{p}^n; t)$ are coupled together by a set of equations called the BBGKY hierarchy. A similar hierarchy exists for the equilibrium particle densities, assuming again that the forces between particles are pairwise additive; this is generally known as the Yvon–Born–Green or YBG hierarchy.

Consider first the case when $n = 1$. At equilibrium (2.1.20) becomes

$$\begin{aligned} &\left(\frac{\mathbf{p}_1}{m} \cdot \frac{\partial}{\partial \mathbf{r}_1} + \mathbf{X}_1 \cdot \frac{\partial}{\partial \mathbf{p}_1} \right) f_0^{(1)}(\mathbf{r}_1, \mathbf{p}_1) \\ &\quad = -\iint \mathbf{F}_{12} \cdot \frac{\partial}{\partial \mathbf{p}_1} f_0^{(2)}(\mathbf{r}_1, \mathbf{p}_1, \mathbf{r}_2, \mathbf{p}_2)\, \mathrm{d}\mathbf{r}_2\, \mathrm{d}\mathbf{p}_2 \end{aligned} \tag{4.2.1}$$

where, from the expression for $f_0^{(n)}$ given by (2.5.1) with the subscript N omitted:

$$f_0^{(1)}(\mathbf{r}_1, \mathbf{p}_1) = \rho^{(1)}(\mathbf{r}_1) f_{\mathrm{M}}(\mathbf{p}_1) \tag{4.2.2}$$

and

$$f_0^{(2)}(\mathbf{r}_1, \mathbf{p}_1, \mathbf{r}_2, \mathbf{p}_2) = \rho^{(2)}(\mathbf{r}_1, \mathbf{r}_2) f_{\mathrm{M}}(\mathbf{p}_1) f_{\mathrm{M}}(\mathbf{p}_2) \tag{4.2.3}$$

On inserting (4.2.2) and (4.2.3) into (4.2.1), exploiting the normalisation (2.1.27) and the fact that $(\partial/\partial \mathbf{p}) f_{\mathrm{M}}(\mathbf{p}) = -(\beta/m)\mathbf{p} f_{\mathrm{M}}(\mathbf{p})$, and finally dividing

through by $(\beta/m)f_{\mathrm{M}}(\mathbf{p}_1)$, we obtain a relation between the single-particle $(n=1)$ and pair $(n=2)$ densities:

$$(k_{\mathrm{B}}T\mathbf{p}_1\cdot\nabla_1-\mathbf{p}_1\cdot\mathbf{X}_1)\rho^{(1)}(\mathbf{r}_1)=\int(\mathbf{p}_1\cdot\mathbf{F}_{12})\rho^{(2)}(\mathbf{r}_1,\mathbf{r}_2)\,\mathrm{d}\mathbf{r}_2 \tag{4.2.4}$$

Equation (4.2.4) may be cast in the form $\mathbf{p}_i\cdot\mathbf{Q}=0$ where $i=1$, but because this result would be true for any choice of $\mathbf{p}_i$ it follows that $\mathbf{Q}=0$. Thus, replacing the forces $\mathbf{X}_1$ and $\mathbf{F}_{12}$ in (4.2.4) by the negative gradients of the external potential $\phi(\mathbf{r}_1)$ and interparticle potential $v(\mathbf{r}_1,\mathbf{r}_2)$, respectively, and dividing through by $\rho^{(1)}(\mathbf{r}_1)$, we find that

$$-k_{\mathrm{B}}T\nabla_1\ln\rho^{(1)}(\mathbf{r}_1)=\nabla_1\phi(\mathbf{r}_1)+\int\nabla_1 v(\mathbf{r}_1,\mathbf{r}_2)\rho^{(1)}(\mathbf{r}_2)g^{(2)}(\mathbf{r}_1,\mathbf{r}_2)\,\mathrm{d}\mathbf{r}_2 \tag{4.2.5}$$

This expression provides a possible starting point for the calculation of the density profile of a fluid in an external field, while if there are no interactions between particles it reduces to the usual barometric law, $\rho^{(1)}(\mathbf{r})\propto\exp[-\beta\phi(\mathbf{r})]$.

Similar manipulations for the case when $n=2$ yield a relationship between the pair and triplet distribution functions which, in the absence of an external field, takes the form

$$\begin{aligned}&-k_{\mathrm{B}}T\nabla_1\ln g^{(2)}(\mathbf{r}_1,\mathbf{r}_2)\\&=\nabla_1 v(\mathbf{r}_1,\mathbf{r}_2)+\rho\int\nabla_1 v(\mathbf{r}_1,\mathbf{r}_3)\left(\frac{g^{(3)}(\mathbf{r}_1,\mathbf{r}_2,\mathbf{r}_3)}{g^{(2)}(\mathbf{r}_1,\mathbf{r}_2)}-g^{(2)}(\mathbf{r}_1,\mathbf{r}_3)\right)\mathrm{d}\mathbf{r}_3\end{aligned} \tag{4.2.6}$$

where on the right-hand side we have subtracted a term that vanishes in the isotropic case. We now eliminate the triplet distribution function by use of Kirkwood's *superposition approximation*,[1] i.e.

$$g^{(3)}(\mathbf{r}_1,\mathbf{r}_2,\mathbf{r}_3)\approx g^{(2)}(\mathbf{r}_1,\mathbf{r}_2)g^{(2)}(\mathbf{r}_2,\mathbf{r}_3)g^{(2)}(\mathbf{r}_3,\mathbf{r}_1) \tag{4.2.7}$$

which becomes exact in the limit $\rho\to 0$. When this approximation is introduced into (4.2.6) the result is a non-linear integro–differential equation for the pair distribution function in terms of the pair potential:

$$\begin{aligned}&-k_{\mathrm{B}}T\nabla_1[\ln g(\mathbf{r}_1,\mathbf{r}_2)+\beta v(\mathbf{r}_1,\mathbf{r}_2)]\\&=\rho\int\nabla_1 v(\mathbf{r}_1,\mathbf{r}_3)g(\mathbf{r}_2,\mathbf{r}_3)[g(\mathbf{r}_3,\mathbf{r}_1)-1]\,\mathrm{d}\mathbf{r}_3\end{aligned} \tag{4.2.8}$$

This is the Born–Green equation.[2] Given $v(r)$, (4.2.8) can be solved numerically to yield $g(r)$, from which in turn all thermodynamic properties can be derived via the energy, pressure and compressibility equations. The work of Born and Green represented one of the earliest attempts to determine the structure and

thermodynamics of a classical fluid by following a well-defined statistical mechanical route, but the results obtained are satisfactory only at low densities.[3] As we shall see later, other approximate integral equations have subsequently been proposed that work well even at high densities.

By construction, the superposition approximation satisfies the so-called core condition for hard-core systems, meaning that $g^{(3)}(\mathbf{r}_1, \mathbf{r}_2, \mathbf{r}_3)$ vanishes when any of the interparticle distances r_{12}, r_{13}, or r_{23} is less than the hard-core diameter. However, it violates the sum rule

$$g^{(2)}(\mathbf{r}_1, \mathbf{r}_2) = \frac{\rho}{N-2} \int g^{(3)}(\mathbf{r}_1, \mathbf{r}_2, \mathbf{r}_3)\, \mathrm{d}\mathbf{r}_3 \tag{4.2.9}$$

which follows directly from the definitions (2.5.3) and (2.5.9). An alternative to (4.2.7) is provided by the 'convolution' approximation,[4] which has the merit of satisfying (4.2.9) exactly. The approximation is most easily expressed in $\mathbf{k}$-space, where it takes the form

$$S^{(3)}(\mathbf{k}, \mathbf{k}') \equiv \left\langle \frac{1}{N} \rho_{\mathbf{k}} \rho_{\mathbf{k}'} \rho_{-\mathbf{k}-\mathbf{k}'} \right\rangle \approx S(k) S(k') S(|\mathbf{k} + \mathbf{k}'|) \tag{4.2.10}$$

The product of structure factors in (4.2.10) transforms in $\mathbf{r}$-space into a convolution product of pair distribution functions, but this fails to satisfy the core condition and in practice is rarely used. The convolution approximation can be derived[5] by setting the triplet function $\hat{c}^{(3)}(\mathbf{k}, \mathbf{k}')$ equal to zero in the three-particle analogue of the Ornstein–Zernike relation (3.5.10).

4.3 FUNCTIONAL EXPANSIONS AND INTEGRAL EQUATIONS

A series of approximate integral equations for the pair distribution function of a uniform fluid in which the particles interact through pairwise–additive forces can be derived systematically by an elegant method due to Percus.[6] The basis of the method is the interpretation of the quantity $\rho g(r)$ as the single-particle density at a point $\mathbf{r}$ in the fluid when a particle of the system is known to be located at the origin, $\mathbf{r} = 0$. The particle at the origin, labelled 0, is assumed to be fixed in space, while the other particles move in the force field of particle 0. Then the total potential energy of the remaining particles in the 'external' field due to particle 0 is of the form (3.1.3), with

$$\phi(i) = v(0, i) \tag{4.3.1}$$

Let $\Xi[\phi]$, as given by (3.1.8), be the grand partition function in the presence of the external field. In that expression, V_N is the total interatomic potential energy of particles $1, \ldots, N$. Alternatively, we may treat the particle at the

origin as an $(N+1)$th particle. Then

$$V_N + \sum_{i=1}^{N} \phi(i) = \sum_{i=1}^{N} \sum_{j>i}^{N} v(i,j) + \sum_{i=1}^{N} v(0,i) = V_{N+1} \tag{4.3.2}$$

If we denote the partition function in the absence of the field by Ξ_0, (3.1.8) can be rewritten as

$$\begin{aligned} \Xi[\phi] &= \sum_{N=0}^{\infty} \frac{z^N}{N!} \int \cdots \int \exp(-\beta V_{N+1})\, \mathrm{d}1 \cdots \mathrm{d}N \\ &= \frac{\Xi_0}{z} \sum_{N=0}^{\infty} \frac{1}{\Xi_0} \frac{z^{N+1}}{N!} \int \cdots \int \exp(-\beta V_{N+1})\, \mathrm{d}1 \cdots \mathrm{d}N \\ &= \frac{\Xi_0}{z} \sum_{N=1}^{\infty} \frac{1}{\Xi_0} \frac{z^N}{(N-1)!} \int \cdots \int \exp(-\beta V_N)\, \mathrm{d}1 \cdots \mathrm{d}(N-1) \end{aligned} \tag{4.3.3}$$

Equation (2.5.3) shows that the sum on N in (4.3.3) is the definition of the single-particle density in a homogeneous system. Thus

$$\Xi[\phi] = \frac{\rho \Xi_0}{z} \tag{4.3.4}$$

The physical content of this result is closely related to that of (2.4.30). By a similar manipulation, but starting from (3.1.9), it can be shown that the single-particle density in the presence of the external field is related to the two-particle density in the absence of the field by

$$\rho^{(1)}(1|\phi) = \frac{\rho^{(2)}(0,1|\phi=0)}{\rho} \tag{4.3.5}$$

Because the system is spatially uniform in the absence of the field, (2.6.7) and (4.3.5) together yield the relation

$$\rho^{(1)}(1|\phi) = \rho g(0,1) \tag{4.3.6}$$

which is the mathematical expression of Percus's idea. The effect of switching on the force field of particle 0 is to change the potential $\phi(1)$ from zero to $\Delta\phi = v(0,1)$; the response, measured by the change in the single-particle density, is

$$\Delta\rho^{(1)}(1) = \rho^{(1)}(1|\phi) - \rho^{(1)}(1|\phi=0) = \rho g(0,1) - \rho = \rho h(0,1) \tag{4.3.7}$$

If the field due to particle 0 is regarded as a perturbation it is natural to consider functional Taylor expansions of various functionals of ϕ or $\rho^{(1)}$ with respect to $\Delta\phi$. One obvious choice is to expand $\Delta\rho^{(1)}$ itself in powers of $\Delta\phi$. The first-order result is simply the Yvon equation (3.6.7), with the infinitesimal quantities $\delta\rho^{(1)}, \delta\phi$ replaced by $\Delta\rho^{(1)}, \Delta\phi$. On combining this expression with (4.3.1) and (4.3.7) we find that

$$h(0,1) = -\beta v(0,1) + \rho \int h(1,2)[-\beta v(0,2)]\,\mathrm{d}2 \tag{4.3.8}$$

Comparison with the Ornstein–Zernike relation (3.5.12) shows that in this approximation

$$c(0,1) \approx -\beta v(0,1) \tag{4.3.9}$$

When the potential is steeply repulsive at short range, (4.3.8) and (4.3.9) are very poor approximations, because $\Delta\rho^{(1)}$ is then a highly non-linear functional of ϕ. The approach is more successful in the case of the Coulomb potential; as we shall see in Section 4.5, (4.3.9) is equivalent to the Debye–Hückel approximation.

Better results are obtained for short-ranged potentials by expansion in powers of $\Delta\rho^{(1)}$. In combination with the Ornstein–Zernike relation, each choice of functional to be expanded yields a different integral equation for the pair distribution function. Here we consider the effect of expanding the intrinsic free energy. Equation (3.5.23) is an exact relation for $\mathcal{F}^{\mathrm{ex}}[\rho^{(1)}]$ relative to the free energy of a reference system at the same temperature and chemical potential. If we take the reference system to be a uniform fluid of density ρ_0 and chemical potential μ_0, the quantities $c_0^{(1)}, \mathcal{F}^{\mathrm{ex}}$ can be replaced by $-\beta\mu_0^{\mathrm{ex}}$, F_0^{ex} and (3.5.23) becomes

$$\begin{aligned}\mathcal{F}^{\mathrm{ex}}[\rho^{(1)}] = F_0^{\mathrm{ex}} + \mu_0^{\mathrm{ex}} \int \Delta\rho^{(1)}(\mathbf{r})\,\mathrm{d}\mathbf{r} \\ - k_{\mathrm{B}}T \int_0^1 \mathrm{d}\lambda(1-\lambda) \iint \Delta\rho^{(1)}(\mathbf{r})c^{(2)}(\mathbf{r},\mathbf{r}';\lambda)\Delta\rho^{(1)}(\mathbf{r}')\mathrm{d}\mathbf{r}\,\mathrm{d}\mathbf{r}'\end{aligned} \tag{4.3.10}$$

This result is still exact, but if we make the approximation of setting $c^{(2)}(\mathbf{r},\mathbf{r}';\lambda)$ equal to the direct correlation function of the reference system, $c_0^{(2)}(\mathbf{r},\mathbf{r}')$, for all values of λ, we obtain an expansion of $\mathcal{F}^{\mathrm{ex}}[\rho^{(1)}]$ correct to second order in $\Delta\rho^{(1)} \equiv \rho^{(1)} - \rho_0$:

$$\begin{aligned}\mathcal{F}^{\mathrm{ex}} \approx F_0^{\mathrm{ex}} + \mu_0^{\mathrm{ex}} \int \Delta\rho^{(1)}(\mathbf{r})\mathrm{d}\mathbf{r} \\ -\frac{1}{2}k_{\mathrm{B}}T \iint \Delta\rho^{(1)}(\mathbf{r})c_0^{(2)}(\mathbf{r},\mathbf{r}')\Delta\rho^{(1)}(\mathbf{r}')\mathrm{d}\mathbf{r}\,\mathrm{d}\mathbf{r}'\end{aligned} \tag{4.3.11}$$

or, after adding the ideal part (3.1.22) and replacing μ_0^{ex} by $\mu_0 - k_B T \ln \Lambda^3 \rho_0$:

$$\mathcal{F}[\rho^{(1)}] \approx F_0 + (\mu_0 - k_B T) \int \Delta\rho^{(1)}(\mathbf{r})\mathrm{d}\mathbf{r} + k_B T \int \rho^{(1)}(\mathbf{r}) \ln \frac{\rho^{(1)}(\mathbf{r})}{\rho_0} \mathrm{d}\mathbf{r} - \frac{1}{2} k_B T \iint \Delta\rho^{(1)}(\mathbf{r}) c_0^{(2)}(|\mathbf{r} - \mathbf{r}'|) \Delta\rho^{(1)}(\mathbf{r}') \mathrm{d}\mathbf{r}\, \mathrm{d}\mathbf{r}' \tag{4.3.12}$$

The grand potential functional $\Omega_\phi[\rho^{(1)}]$ defined by (3.4.1) is

$$\Omega_\phi[\rho^{(1)}] = \mathcal{F}[\rho^{(1)}] + \int \rho^{(1)}(\mathbf{r})\phi(\mathbf{r})\mathrm{d}\mathbf{r} - \mu \int \rho^{(1)}(\mathbf{r})\mathrm{d}\mathbf{r} \tag{4.3.13}$$

or, after substitution for $\mathcal{F}$ from (4.3.12):

$$\Omega_\phi[\rho^{(1)}] \approx \Omega_0 + \int \rho^{(1)}(\mathbf{r})\phi(\mathbf{r})\mathrm{d}\mathbf{r} + k_B T \int \left(\rho^{(1)}(\mathbf{r}) \ln \frac{\rho^{(1)}(\mathbf{r})}{\rho_0} - \Delta\rho^{(1)}(\mathbf{r}) \right) \mathrm{d}\mathbf{r} - \frac{1}{2} k_B T \iint \Delta\rho^{(1)}(\mathbf{r}) c_0^{(2)}(|\mathbf{r} - \mathbf{r}'|) \Delta\rho^{(1)}(\mathbf{r}') \mathrm{d}\mathbf{r}\, \mathrm{d}\mathbf{r}' \tag{4.3.14}$$

where

$$\Omega_0 = F_0 - \mu_0 \int \rho_0 \, \mathrm{d}\mathbf{r} \tag{4.3.15}$$

is the grand potential of the reference system. At equilibrium, Ω_ϕ is a minimum with respect to variations in the single-particle density, and it is straightforward to show that the density that minimises (4.3.14) is

$$\rho^{(1)}(\mathbf{r}) = \rho_0 \exp\left(-\beta\phi(\mathbf{r}) + \int \Delta\rho^{(1)}(\mathbf{r}') c_0^{(2)}(|\mathbf{r} - \mathbf{r}'|) \, \mathrm{d}\mathbf{r}' \right) \tag{4.3.16}$$

The same result is obtained by minimising the total free-energy functional obtained by adding the external field term to (4.3.12), but subject now to the constraint that the total number of particles must remain constant, i.e.

$$\int \Delta\rho^{(1)}(\mathbf{r}) \, \mathrm{d}\mathbf{r} = 0 \tag{4.3.17}$$

Equation (4.3.16) may be interpreted either as an expression for the density profile of a fluid in a true external field or, following Percus, as an expression for the pair distribution function of a uniform fluid of density ρ_0, when $\phi(r)$ can be identified with the pair potential. In the uniform case it follows from (4.3.7) that

$$g(\mathbf{r}) = \exp\left(-\beta v(\mathbf{r}) + \rho \int c(|\mathbf{r} - \mathbf{r}'|) h(\mathbf{r}') \, \mathrm{d}\mathbf{r}' \right) \tag{4.3.18}$$

or, from the Ornstein–Zernike relation (3.5.12):

$$g(\mathbf{r}) = \exp[-\beta v(\mathbf{r})] \exp[h(\mathbf{r}) - c(\mathbf{r})] \tag{4.3.19}$$

This is the *hypernetted chain* or HNC approximation.[7] The corresponding expression for the grand potential is obtained by substituting (4.3.16) for $\rho^{(1)}(\mathbf{r})$ in (4.3.14). The result, after some rearrangement and use of the Ornstein–Zernike relation and of (4.3.7), is

$$\Omega = \Omega_0 + \frac{1}{2}\rho k_B T \int h(\mathbf{r})[h(\mathbf{r}) - c(\mathbf{r})]\, d\mathbf{r} - \rho k_B T \int c(\mathbf{r})\, d\mathbf{r} \tag{4.3.20}$$

The quantity $\Delta\Omega = \Omega - \Omega_0$ is the change in grand potential arising from the introduction of a particle that acts as the source of the external field. Since that particle is fixed in space, it makes no contribution to the ideal free energy, and the change in grand potential is therefore equal to the excess chemical potential. Thus, in the HNC approximation:

$$\beta\mu^{ex} = \frac{1}{2}\rho \int h(\mathbf{r})[h(\mathbf{r}) - c(\mathbf{r})]\, d\mathbf{r} - \rho \int c(\mathbf{r})\, d\mathbf{r} \tag{4.3.21}$$

Equation (4.3.19) represents an approximate closure of the Ornstein–Zernike relation, since it provides a second, independent relation between $h(r)$ and $c(r)$. Elimination of $c(r)$ between the two relations yields the HNC integral equation:

$$\ln g(\mathbf{r}) + \beta v(\mathbf{r}) = \rho \int [g(\mathbf{r} - \mathbf{r}') - 1][g(\mathbf{r}') - 1 - \ln g(\mathbf{r}') - \beta v(\mathbf{r}')]\, d\mathbf{r}' \tag{4.3.22}$$

Equation (4.3.22) and other integral equations of a similar type can be solved numerically by an iterative approach, starting with a guess for either of the functions h or c. Perhaps the easiest method is to use the relation (3.5.13) between the Fourier transforms of h and c. An initial guess, $c_{(0)}(r)$ say, is made and its Fourier transform inserted in (3.5.13); an inverse transformation yields a first approximation for $h(r)$. The closure relation between h and c is then used to obtain an improved guess, $c_{(1)}(r)$ say. The process is repeated, with $c_{(1)}(r)$ replacing $c_{(0)}(r)$ as input, and the iteration continues until convergence is achieved.[8] To ensure convergence it is generally necessary to mix successive approximations to $c(r)$ before they are used at the next level of iteration. A variety of elaborations of this basic scheme have been worked out, based on a decomposition of $h - c$ into coarse and fine parts and use of the Newton–Raphson algorithm to solve the integral equation on the coarse grid.[8]

Use of (4.3.19) is equivalent to setting

$$c(\mathbf{r}) = h(\mathbf{r}) - \ln[h(\mathbf{r}) + 1] - \beta v(\mathbf{r}) \tag{4.3.23}$$

For sufficiently large r, $h(r) \ll 1$; if we expand the logarithmic term in (4.3.23), we find that $c(r) \approx -\beta v(r)$. As we shall see in Chapter 10, the r^{-1} decay

of $c(r)$ at large r is crucial in determining the properties of ionic fluids. For such systems we must expect the HNC approximation to be superior to those approximations in which $c(r)$ has a different asymptotic behaviour.

4.4 THE PERCUS–YEVICK EQUATION

The derivation of (4.3.19) has a strong appeal, since it shows that the HNC closure of the Ornstein–Zernike relation corresponds to minimising a well-defined grand potential (or free energy) functional, albeit an approximate one. It also leads naturally to an expression for the chemical potential of a uniform fluid expressed solely in terms of the functions $h(r)$ and $c(r)$. The HNC equation can, however, be derived in a simpler way by expanding the single-particle direct correlation function $c^{(1)}(\mathbf{r})$ of an inhomogeneous fluid about that of a uniform reference system in powers of $\Delta\rho^{(1)}$ where, as before, we follow Percus's idea by supposing that the inhomogeneity is induced by 'switching on' the interaction $\phi(\mathbf{r})$ with a particle fixed at the origin. To first order in $\Delta\rho^{(1)}$ the result is

$$\begin{aligned} c^{(1)}(\mathbf{r}) &\approx c_0^{(1)} + \int \Delta\rho^{(1)}(\mathbf{r}') \left.\frac{\delta c^{(1)}(\mathbf{r})}{\delta\rho^{(1)}(\mathbf{r}')}\right|_{\phi=0} \mathrm{d}\mathbf{r}' \\ &= -\beta\mu_0^{\mathrm{ex}} + \int \Delta\rho^{(1)}(\mathbf{r}')c_0^{(2)}(\mathbf{r},\mathbf{r}')\,\mathrm{d}\mathbf{r}' \end{aligned} \tag{4.4.1}$$

where the subscript 0 again denotes a property of the reference system. When taken together with the relation (3.5.4) between $c^{(1)}(\mathbf{r})$ and $\rho^{(1)}(\mathbf{r})$, it is easy to show that (4.4.1) is equivalent to (4.3.16), and therefore leads again to the HNC expression (4.3.19). This method of approach is also suggestive of routes to other integral equation approximations, since there are many functionals that could be expanded to yield a possibly useful closure of the Ornstein–Zernike relation. We can, for example, choose to expand $\exp[c^{(1)}(\mathbf{r})]$ in powers of $\Delta\rho^{(1)}$. The first-order result is now

$$\begin{aligned} \exp[c^{(1)}(\mathbf{r})] &\approx \exp\left(-\beta\mu_0^{\mathrm{ex}}\right) + \int \Delta\rho^{(1)}(\mathbf{r}') \left.\frac{\delta \exp[c^{(1)}(\mathbf{r})]}{\delta\rho^{(1)}(\mathbf{r}')}\right|_{\phi=0} \mathrm{d}\mathbf{r}' \\ &= \exp\left(-\beta\mu_0^{\mathrm{ex}}\right)\left(1 + \int \Delta\rho^{(1)}(\mathbf{r}')c_0^{(2)}(\mathbf{r},\mathbf{r}')\,\mathrm{d}\mathbf{r}'\right) \end{aligned} \tag{4.4.2}$$

which leads, via (3.5.4), to an expression for the pair distribution function of a uniform fluid:

$$\begin{aligned} g(\mathbf{r}) &= \exp[-\beta v(\mathbf{r})]\left(1 + \rho\int c(|\mathbf{r}-\mathbf{r}'|)h(\mathbf{r}')\,\mathrm{d}\mathbf{r}'\right) \\ &= \exp[-\beta v(\mathbf{r})][1 + h(\mathbf{r}) - c(\mathbf{r})] \end{aligned} \tag{4.4.3}$$

This is the Percus–Yevick or PY approximation.[9] The integral equation that results from using the Ornstein–Zernike relation to eliminate $c(\mathbf{r})$ from (4.4.3) is

$$\exp[\beta v(\mathbf{r})]g(\mathbf{r}) = 1+\rho\int[g(\mathbf{r}-\mathbf{r}')-1]g(\mathbf{r}')\left(1-\exp[\beta v(\mathbf{r}')]\right)\mathrm{d}\mathbf{r}' \quad (4.4.4)$$

The approximation (4.4.3) is equivalent to taking

$$c(\mathbf{r}) \approx \left(1-\exp[\beta v(\mathbf{r})]\right)g(\mathbf{r}) = g(\mathbf{r}) - y(\mathbf{r}) \quad (4.4.5)$$

where $y(r)$ is the cavity distribution function defined by (2.5.23). It follows that $c(\mathbf{r})$ is assumed to vanish wherever the potential is zero. The PY equation has proved to be more successful than the HNC approximation when the potential is strongly repulsive and short ranged. From comparison of (4.4.3) with (4.3.19) we see that the PY approximation is recovered by linearisation of the HNC result with respect to $(h-c)$, while a diagrammatic analysis shows that the PY equation corresponds to summing a smaller class of diagrams in the density expansion of $h(r)$. To some extent, therefore, the greater success of the PY equation in the case of short-range potentials must be due to a cancellation of errors.

The HNC and PY equations are the classic integral equation approximations of liquid state theory. We shall deal shortly with the question of their quantitative reliability, but it is useful initially to note some general features of the two approximations. Both equations predict, correctly, that $g(r)$ behaves as $\exp[-\beta v(r)]$ in the limit $\rho \to 0$. As we shall see in Section 4.6, they also yield the correct expression for the term of order ρ in the density expansion of $g(r)$. It follows that they both give the correct second and third virial coefficients in the density expansion of the equation of state. At order ρ^2 and beyond, each approximation neglects a certain number (different for each theory) of the diagrams appearing in the exact expansion of $g(r)$. Once a solution for the pair distribution function has been obtained, the internal energy, pressure and compressibility can be calculated from (2.5.20), (2.5.22) and (2.6.12), respectively. The pressure may also be determined in two other ways. First, the inverse compressibility can be integrated numerically with respect to density to yield the so-called compressibility equation of state. Secondly, the internal energy can be integrated with respect to inverse temperature to give the Helmholtz free energy (see (2.3.9)); the latter can in turn be differentiated numerically with respect to volume to give the 'energy' equation of state. The results obtained via the three routes (virial, compressibility and energy) are in general different, sometimes greatly so. This lack of thermodynamic consistency is a common feature of approximate theories. The HNC equation is a special case insofar as it corresponds to a well-defined free energy functional, and differentiation of that free energy with respect to volume can be shown[10] to give the same result as the virial equation. The energy and virial routes to the equation of state are therefore equivalent.

The PY equation (4.4.4) is of particular interest in the theory of simple liquids because it is soluble analytically in the important case of the hard-sphere fluid. Written in terms of the function $y(r)$, the PY approximation (4.4.5) is

$$c(r) = y(r)f(r) \tag{4.4.6}$$

For hard spheres of diameter d, (4.4.6) is equivalent to setting

$$\begin{aligned} c(r) &= -y(r), \quad r < d \\ &= 0, \qquad r > d \end{aligned} \tag{4.4.7}$$

It follows that $c(r)$ has a discontinuity at $r = d$, since $y(r)$ is continuous everywhere (see below in Section 4.6). The solution is further restricted by the fact that $g(r)$ must vanish inside the hard core, i.e.

$$g(r) = 0, \quad r < d \tag{4.4.8}$$

Given (4.4.7) and (4.4.8) it is possible to rewrite the PY equation as an integral equation for $y(r)$ in the form

$$y(r) = 1 + \rho \int_{r'<d} y(r')\,\mathrm{d}\mathbf{r}' - \rho \int_{\substack{r'<d \\ |\mathbf{r}-\mathbf{r}'|>d}} y(r')y(|\mathbf{r}-\mathbf{r}'|)\,\mathrm{d}\mathbf{r}' \tag{4.4.9}$$

which was solved independently by Thiele and Wertheim by use of Laplace transform methods.[11] The final result for $c(r)$ is

$$\begin{aligned} c(x) &= -\lambda_1 - 6\eta\lambda_2 x - \frac{1}{2}\eta\lambda_1 x^3, \quad x < 1 \\ &= 0, \qquad\qquad\qquad\qquad\quad x > 1 \end{aligned} \tag{4.4.10}$$

where $x = r/d$, η is the packing fraction and

$$\lambda_1 = (1+2\eta)^2/(1-\eta)^4, \qquad \lambda_2 = -(2+\eta)^2/4(1-\eta)^4 \tag{4.4.11}$$

Appendix D describes a different method of solution, due to Baxter[12]; this has the advantage of being easily generalised to cases where the potential consists of a hard-sphere core and a tail.

The compressibility of the hard-sphere fluid is obtained by substitution of (4.4.10) in (3.5.15), and integration with respect to η yields the compressibility equation of state:

$$\frac{\beta P^{\mathrm{c}}}{\rho} = \frac{1+\eta+\eta^2}{(1-\eta)^3} \tag{4.4.12}$$

Alternatively, substitution of

$$\lim_{r\to d^+} g(r) = y(d) = -\lim_{r\to d^-} c(r) \tag{4.4.13}$$

in (2.5.26) leads to the virial equation of state:

$$\frac{\beta P^{\mathrm{v}}}{\rho} = \frac{1 + 2\eta + 3\eta^2}{(1-\eta)^2} \tag{4.4.14}$$

The difference between P^{c} and P^{v} increases with increasing density. The general expressions for the nth virial coefficient, obtained by expanding the two equations in powers of η, are

$$\begin{aligned} B_n^{\mathrm{c}}/b^{n-1} &= 2[2 + 3n(n-1)]/4^n \\ B_n^{\mathrm{v}}/b^{n-1} &= 8[3n-4]/4^n \end{aligned} \tag{4.4.15}$$

where $b \equiv B_2 = (2\pi/3)d^3$. Both equations yield the exact values of B_2 and B_3 but give incorrect (and different) values for the higher-order coefficients.

The full equations of state are plotted in Figure 4.2 for comparison with results predicted by the Carnahan–Starling formula (3.9.20), which is nearly exact. The pressures calculated from the compressibility equation lie systematically closer to and above the Carnahan–Starling results at all densities, while the virial pressures lie below them. It appears that the Carnahan–Starling formula interpolates accurately between the two PY expressions; in fact

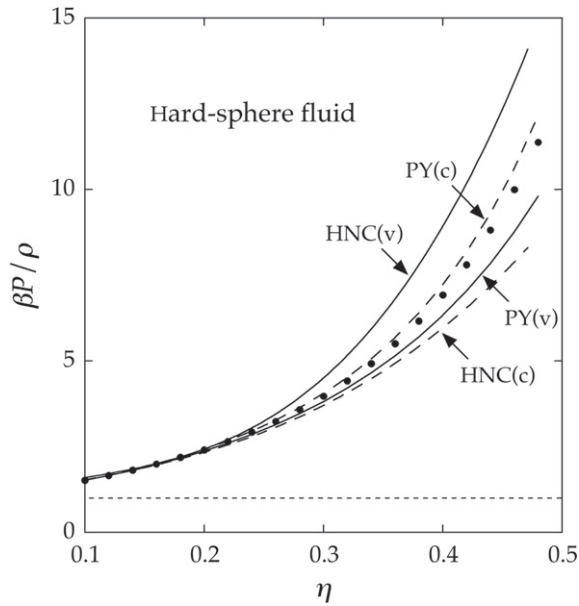

FIGURE 4.2 Equation of state of the hard-sphere fluid in the PY and HNC approximations. The full curves and dashes show results from the virial and compressibility equations, respectively, and the points are results obtained from the Carnahan–Starling equation (3.9.20).

(3.9.20) is recovered if (4.4.12) and (4.4.14) are added together with weights, respectively, of two-thirds and one-third:

$$\frac{\beta P}{\rho} = \frac{\beta}{3\rho}(2P^{c} + P^{v}) = \frac{1 + \eta + \eta^2 - \eta^3}{(1-\eta)^3} \tag{4.4.16}$$

The compressibility and virial equations of state obtained by numerical solution of the HNC equation are also shown in Figure 4.2. They are clearly inferior to their PY counterparts.

The Thiele–Wertheim solution of the PY equation was later extended to the case of binary mixtures of additive hard spheres by Lebowitz and Rowlinson.[13] Their results show that the two components should be miscible in all proportions irrespective of diameter ratio. It is therefore understandable that the same conclusion follows from the BMLCS equation (3.10.12), since this can be derived by weighting the PY expressions for the compressibility and virial equations of state of the mixture in a manner identical to the first equality in (4.4.16).

The PY approximation to the pair distribution function is obtained by substitution of (4.4.10) into the Ornstein–Zernike relation; as a consequence of the discontinuity in $c(r)$ at $r = d$, $g(r)$ is only a piecewise–analytical function.[14] A comparison of the calculated distribution function with the results of a Monte Carlo simulation of the hard-sphere fluid at a density ($\eta = 0.49$) close to the fluid–solid transition is shown in Figure 4.3. Although the general agreement is good, the theoretical curve shows two significant defects. First, the value at contact is too low. Secondly, the oscillations are slightly out of phase with the Monte Carlo results. In addition, the amplitude of the oscillations decreases too slowly with increasing distance, with the consequence that the main peak in the structure factor is too high, reaching a maximum value of 3.05 rather than the value 2.85 obtained by simulation. An accurate representation of the pair distribution function of the hard-sphere fluid is an important ingredient of many theories. To meet that need, a simple, semi-empirical modification of the PY result has been devised in which the faults seen in Figure 4.3 are corrected.[15]

An analytical solution of the PY equation has also been derived for the 'sticky sphere' model of Baxter[16] along the lines followed for hard spheres in Appendix D. The model is one that corresponds to the square-well potential of Figure 1.2 in the limit of vanishing range of attraction ($\gamma \to 1^{+}$) and divergent well depth ($\epsilon \to \infty$):

$$\begin{aligned} \beta v(r) &= \infty, && r < d \\ &= \ln\left[\frac{12\tau(\gamma-1)}{\gamma d}\right], && d \le r < \gamma d,\ \gamma \to 1^{+} \\ &= 0, && r > \gamma d \end{aligned} \tag{4.4.17}$$

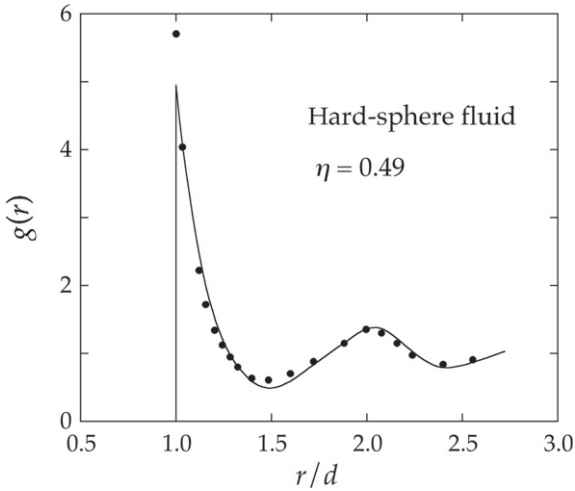

FIGURE 4.3 Radial distribution function of the hard-sphere fluid at a density close to the fluid–solid transition. The curve shows the PY solution and the points are the results of Monte Carlo calculations.

The quantity τ is a dimensionless measure of the temperature that increases monotonically with T, while the form of the attractive term ensures that the second virial coefficent (3.9.7) remains finite:

$$B_2(\tau) = \frac{\pi d^3}{6}\left(4 - \frac{1}{\tau}\right) \tag{4.4.18}$$

The PY solution shows that the model undergoes a first-order, gas–liquid transition below a critical point at $\tau_c = (2-\sqrt{2})/6 \approx 0.0976$ and $\eta_c = (3\sqrt{2}-4)/2 \approx 0.1213$. Sticky spheres provide a useful model of colloidal systems, where the attractive interactions are frequently both strong and very short ranged compared with the particle dimensions.

Solutions to the PY and HNC equations have been obtained for a variety of other pair potentials over wide ranges of temperature and density. Comparison of results for the Lennard-Jones potential with those of computer simulations shows that the PY approximation is superior at all thermodynamic states for which calculations have been made.[3] At high temperatures the agreement with simulations is excellent both for internal energy and for pressure, but it worsens rapidly as the temperature is reduced. Figure 4.4 shows results for the virial and energy equations of state along the isotherm $T^* = 1.35$, which corresponds to a near-critical temperature. Although the pressures calculated by the energy route are in good agreement with those obtained by simulation,[18] the more significant feature of the results is the serious thermodynamic inconsistency that they reveal, which becomes more severe as the temperature is lowered further.

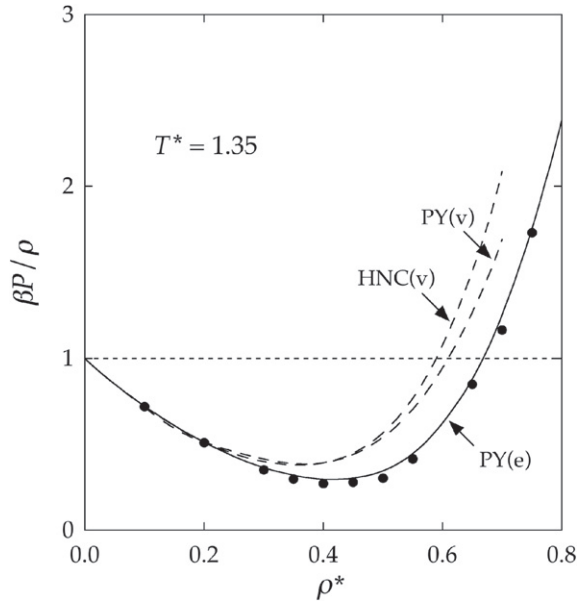

FIGURE 4.4 Equation of state of the Lennard-Jones fluid along the isotherm $T^* = 1.35$. The curves show results obtained from the PY and HNC equations via the virial (v) and energy (e) routes and the points are the results of Monte Carlo calculations.[17]

The deficiencies in the PY approximation at low temperatures are also evident in the behaviour of the pair distribution function. The main peak in $g(r)$ has too great a height and occurs at too small a value of r, while the later oscillations are out of phase with the results of simulations; in the latter respect, the situation is markedly worse than it is for hard spheres. These weaknesses show that the PY approximation cannot be regarded as a quantitatively satisfactory theory of the liquid state.

4.5 THE MEAN SPHERICAL APPROXIMATION

There are a variety of model fluids of interest in the theory of liquids for which the pair potential consists of a hard-sphere interaction plus a tail. The tail is normally attractive, but not necessarily spherically symmetric. Such systems have been widely studied in the *mean spherical approximation* or MSA. The name comes from the fact that the approximation was first proposed as a generalisation of the mean spherical model of Ising spin systems. The general form of the potential in the spherically symmetric case is

$$\begin{aligned} v(r) &= \infty, \qquad r < d \\ &= v_1(r), \quad r > d \end{aligned} \tag{4.5.1}$$

where d is the hard-sphere diameter. The MSA is defined in terms of the pair distribution and direct correlation functions by

$$\begin{aligned} g(r) &= 0, & r < d \\ c(r) &= -\beta v_1(r), & r > d \end{aligned} \tag{4.5.2}$$

When supplemented by the Ornstein–Zernike relation, these two expressions combine to yield an integral equation for $g(r)$. The first expression is exact, while the second extends the asymptotic behaviour of $c(r)$ to all $r > d$ and is clearly an approximation. Despite the crude form assumed for $c(r)$, the MSA gives good results in many cases. For example, it provides a much better description of the properties of the square-well fluid[19] than is given by either the PY or HNC approximation. However, the most attractive feature of the MSA is the fact that the integral equation can be solved analytically for a number of potential models of physical interest, including the hard-core Yukawa fluid defined by (1.2.2) as well as simple models of electrolyte solutions (discussed in Chapter 10) and polar liquids (Chapter 11).

The PY equation for hard spheres is the special case of the MSA when the tail in the potential is absent and the analytical solution of the MSA for certain pair potentials is closely linked to the method of solution of the PY hard-sphere problem. The two theories also have a common diagrammatic structure,[20] but the connection between them can be established more easily in the following way. The basic PY approximation (4.4.3) may be expressed in the form

$$c(r) = f(r) + f(r)[h(r) - c(r)] \tag{4.5.3}$$

where $f(r)$ is the Mayer function for the potential $v(r)$. In the low-density limit, $h(r)$ and $c(r)$ become the same, and the right-hand side of (4.5.3) reduces to $f(r)$. Equation (4.5.3) can therefore be rewritten as

$$c(r) = c_0(r) + f(r)[h(r) - c(r)] \tag{4.5.4}$$

where $c_0(r)$, the limiting value of $c(r)$ at low density, is equal to $f(r)$ both in an exact theory and in the PY approximation. If we choose another form for $c_0(r)$ in (4.5.4), we generate a different theory. For a potential of the type defined by (4.5.1) the exact $c_0(r)$ is

$$c_0(r) = \exp[-\beta v(r)] - 1 = [1 + f_d(r)]\exp[-\beta v_1(r)] - 1 \tag{4.5.5}$$

where $f_d(r)$ is the Mayer function for hard spheres. The MSA is equivalent to linearising (4.5.5) with respect to $v_1(r)$ by setting

$$c_0(r) \approx [1 + f_d(r)][1 - \beta v_1(r)] - 1 = f_d(r) - \beta v_1(r)[1 + f_d(r)] \tag{4.5.6}$$

and at the same time replacing f by f_d in (4.5.4). Taken together, these two approximations give rise to the expression

$$f_d(r)[1 + h(r)] = [c(r) + \beta v_1(r)][1 + f_d(r)] \tag{4.5.7}$$

which is equivalent to the closure relation (4.5.2). This characterisation of the MSA shows that it involves approximations additional to those underlying the PY equation. One would therefore not expect the MSA to be of comparable accuracy to the PY approximation. In practice, as the results for the square-well fluid show, this is not always true.

The structure of (4.5.7) suggests a natural way in which the MSA can be extended to a class of pair potentials wider than that defined by (4.5.1).[21] Let us suppose that the potential $v(r)$ is divided in the form

$$v(r) = v_0(r) + v_1(r) \tag{4.5.8}$$

The conventional MSA applies only when v_0 is the hard-sphere potential. When $v_0(r)$ is strongly repulsive but continuous the natural generalisation of the closure relation (4.5.7) is obtained by replacing f_d by f_0, the Mayer function for the potential v_0. The resulting equation can then be rearranged to give

$$g(r) = \exp[-\beta v_0(r)][1 + h(r) - c(r) - \beta v_1(r)] \tag{4.5.9}$$

which reduces to the PY approximation (4.4.3) when $v_1(r)$ is very weak. When applied to the Lennard-Jones fluid the 'soft-core' MSA gives good results when the potential is divided at its minimum in the manner that has also proved very successful when used in thermodynamic perturbation theory (see Section 5.4).

4.6 DIAGRAMMATIC EXPANSIONS OF THE PAIR FUNCTIONS

In Section 3.8 we derived the density expansion of the two-particle direct correlation function $c^{(2)}(1,2)$. We now wish to do the same for other pair functions. One of our main goals is to obtain a precise, diagrammatic characterisation of the HNC approximation of Section 4.3. The simplest way to proceed is to take as starting point the iterative solution of the Ornstein–Zernike relation in (3.5.11). That solution can be expressed in diagrammatic terms as

$h(1,2)$ = [all chain diagrams consisting of two terminal white 1-circles labelled 1 and 2, black $\rho^{(1)}$-circles and c-bonds]

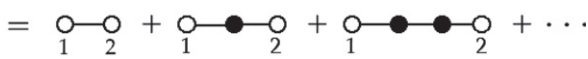

(4.6.1)

where the meaning of the terms 'chain' diagram and 'terminal' circle is self-evident. We now replace the c-bonds in (4.6.1) by their series expansion. The first term on the right-hand side of (4.6.1) yields the complete set of diagrams that contribute to $c(1,2)$ and are therefore free of connecting circles, which means they contain neither articulation circles nor nodal circles. The black circles appearing at higher order are all nodal circles; they remain nodal circles when the c-bonds are replaced by diagrams drawn from the series (3.8.7), but no

articulation circles appear. The topology of the resulting diagrams is therefore similar to that of the diagrams in the series for $c(1,2)$ except that nodal circles are now permitted. Thus[22]

$$h(1,2) = [\text{all irreducible diagrams consisting of two white 1-circles labelled 1 and 2, black } \rho^{(1)}\text{-circles and } f\text{-bonds}] \tag{4.6.2}$$

Equation (4.6.2) contains more diagrams than (3.8.7) at each order in density beyond the zeroth-order term; the additional diagrams contain at least one nodal circle. For example, of the two second-order terms shown below, (a) appears in both expansions but (b) appears only in (4.6.2), because in (b) the black circles are nodal circles:

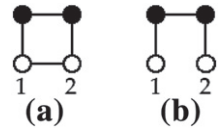

Diagrams (a) and (b) differ only by the presence in (a) of an f-bond between the white circles. If we recall that $e(1,2) = f(1,2) + 1$, we see that the sum of (a) and (b) is given by a single diagram in which the white circles are linked by an e-bond. All diagrams in (4.6.2) can be paired uniquely in this way, except that the lowest-order diagram

appears alone. We therefore add to (4.6.2) the disconnected diagram consisting of two white 1-circles:

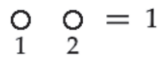

and obtain an expansion of $g(1,2) = h(1,2) + 1$ in terms of diagrams in which the white circles are linked by an e-bond and all other bonds are f-bonds. Alternatively, on dividing through by $e(1,2)$, we find that the cavity distribution function $y(1,2) = g(1,2)/e(1,2)$ can be expressed in the form

$$y(1,2) = [\text{all irreducible diagrams consisting of two non-adjacent white 1-circles labelled 1 and 2, black } \rho^{(1)}\text{-circles and } f\text{-bonds}]$$

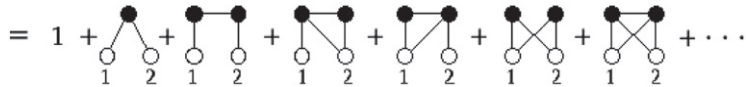

(4.6.3)

If the system is homogeneous and the factor $e(1,2)$ is restored, (4.6.3) becomes an expansion of $g(1,2)$ in powers of ρ with coefficients $g_n(r)$ such that

$$g(r) = \exp[-\beta v(r)]\left(1 + \sum_{n=1}^{\infty} \rho^n g_n(r)\right) \tag{4.6.4}$$

Both $g_1(r)$ and $g_2(r)$ have been evaluated analytically for hard spheres.[23]

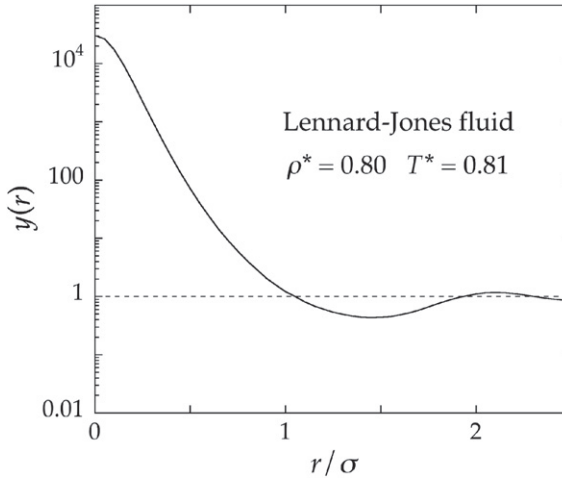

FIGURE 4.5 Monte Carlo results for the cavity distribution function of the Lennard-Jones fluid. After Llano–Restrepo and Chapman.[24]

The form of the series (4.6.4) leads immediately to two important results. First, $g(r)$ behaves as $\exp[-\beta v(r)]$ as $\rho \to 0$, as we proved in a different way in Section 2.6. Secondly, $y(r)$ is a continuous function of r even for hard spheres, for which the discontinuity in $g(r)$ at $r = d$ is wholly contained in the factor $\exp[-\beta v(r)]$. This useful property has already been exploited in the derivation of the hard-sphere equation of state (2.5.26). It is also clear from (4.6.3) that $y(1,2)$ can be interpreted as the distribution function for a pair 1, 2 in a 'mixed' system in which the interaction between those particles is suppressed (and hence $e(1,2) = 1$) but other interactions remain the same. For a system of hard spheres, two such particles would correspond to spheres that can overlap each other, but not other particles, and therefore play a role equivalent to that of spherical cavities of volume equal to that of a hard sphere. Figure 4.5 shows the calculated cavity distribution function for the Lennard-Jones fluid in a high-density, low-temperature thermodynamic state. The very rapid increase in $y(r)$ as $r \to 0$ implies that there is a high probability of finding the two 'cavity' particles at very small separations.[25]

The pair distribution function is sometimes written as

$$g(1,2) = \exp[-\beta\psi(1,2)] \tag{4.6.5}$$

where $\psi(1,2)$ is the *potential of mean force*. The name is justified by the fact that the quantity $-\nabla_1\psi(1,2)$ is the force on particle 1, averaged over all positions of particles $3, 4, \ldots$, with particles 1 and 2 held at $\mathbf{r}_1$ and $\mathbf{r}_2$, respectively. This can be proved[26] by taking the logarithm of both sides of the definition of $g(1,2)$ provided by (2.5.3) and (2.5.8) and differentiating with respect to the coordinates of particle 1. In thermodynamic terms the potential of mean force

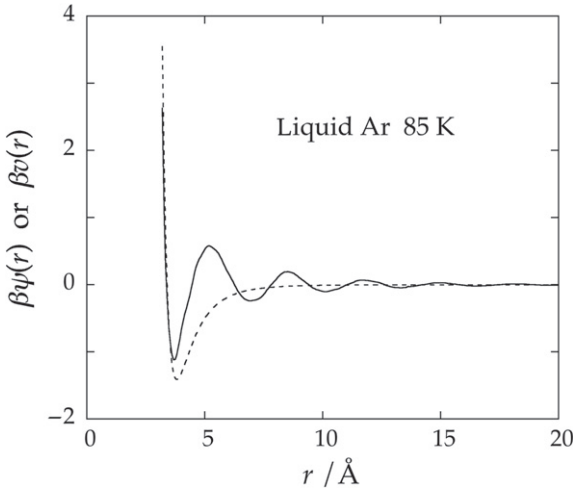

FIGURE 4.6 The full curve shows the potential of mean force for liquid argon at 85 K, derived from the experimental results of Figure 2.3; the dashed curve shows the Lennard-Jones potential with parameters chosen to fit experimental properties of the liquid.

is the reversible work that must be done on the system to bring together at a separation r two particles that initially were infinitely separated. The example plotted in Figure 4.6 is for liquid argon at 85 K, calculated from the experimental neutron scattering results for $g(r)$ shown in Figure 2.3. Depending on the final separation of the particles, the reversible work required may be either positive or negative, with fluctuations that reflect the structure of the liquid.

It is clear from the behaviour of the pair distribution function at low density that $\psi(1,2) \to v(1,2)$ as $\rho \to 0$. If we define a function $\omega(1,2)$ by

$$\omega(1,2) = \beta[v(1,2) - \psi(1,2)] \tag{4.6.6}$$

then

$$g(1,2) = e(1,2)\exp[\omega(1,2)] \tag{4.6.7}$$

and therefore

$$\omega(1,2) = \ln y(1,2) \tag{4.6.8}$$

An application of Lemma 1 of Section 3.7 to the diagrams in (4.6.3) shows that

$$\begin{aligned}\omega(1,2) = [&\text{all diagrams consisting of two non-adjacent white 1-circles}\\ &\text{labelled 1 and 2, black } \rho^{(1)}\text{-circles and } f\text{-bonds, such that}\\ &\text{the white circles are not an articulation pair}]\end{aligned} \tag{4.6.9}$$

The effect of this operation is to eliminate those diagrams in the expansion of $y(1,2)$ that are star products of other diagrams in the same expansion. For

example, it eliminates the penultimate diagram pictured in (4.6.3), since this is the star product of the first diagram with itself:

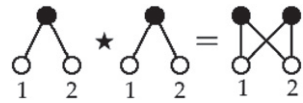

The fact that the white circles in (4.6.9) are not an articulation pair means that there exists at least one path between each pair of black circles which does not pass through either white circle.

From the earlier discussion we know that $c(1,2)$ is the sum of all diagrams in $h(1,2)$ that are free of nodal circles. We therefore define a function $s(1,2)$ such that

$$s(1,2) = h(1,2) - c(1,2) \tag{4.6.10}$$

where

$s(1,2) =$ [all irreducible diagrams consisting of two white 1-circles labelled 1 and 2, black $\rho^{(1)}$-circles and f-bonds, and which contain at least one nodal circle]

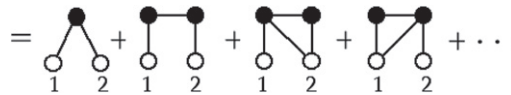

(4.6.11)

Diagrams belonging to the set (4.6.11) are called the *series* diagrams; the function $s(1,2)$ is given by the convolution integral on the right-hand side of the Ornstein–Zernike relation (3.5.10) and is therefore termed the *indirect* correlation function.

All series diagrams are also members of the set (4.6.9). The function $\omega(1,2)$ can therefore be re-expressed as

$$\omega(1,2) = s(1,2) + b(1,2) \tag{4.6.12}$$

where $b(1,2)$ is the sum of the diagrams in (4.6.9) that are free of nodal circles; these are called the *bridge* or *elementary* diagrams and $b(1,2)$ is called the *bridge function*. To second order in density the only bridge diagram is

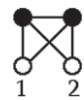

On combining (4.6.7), (4.6.10) and (4.6.12), we obtain the following, exact relation:

$$\ln[h(1,2)+1] = -\beta v(1,2) + b(1,2) + h(1,2) - c(1,2) \tag{4.6.13}$$

Since $h(1,2)$ and $c(1,2)$ are linked by the Ornstein–Zernike relation, (4.6.13) would be transformed into an integral equation for h (or c) if the unknown

function $b(1,2)$ were replaced by some function of h (or c). For example, the f-bond expansion of $b(1,2)$ can be rewritten as an h-bond expansion[27] and inserted in (4.6.13). The result, together with the Ornstein–Zernike relation, constitutes an exact integral equation for $h(1,2)$, but because the h-bond expansion introduces an infinite series of many-dimensional integrals of products of h, the equation is intractable. If instead we set $b(1,2)=0$, we recover the HNC approximation, which was arrived at in a very different way in Section 4.3. By rewriting the exact relation (4.6.13) as

$$y(1,2) = \exp[s(1,2) + b(1,2)] \quad \text{(exact)} \tag{4.6.14}$$

we see that the HNC and PY approximations are equivalent to taking either

$$y(1,2) \approx \exp[s(1,2)] \quad \text{(HNC)} \tag{4.6.15}$$

or

$$y(1,2) \approx s(1,2) + 1 \quad \text{(PY)} \tag{4.6.16}$$

In each case differences with respect to the exact result arise initially only at second order in density. From comparison of (4.6.14) with (4.6.16) it also follows that the PY approximation may be viewed as one for which the bridge function is approximated by

$$b(1,2) \approx \ln[s(1,2) + 1] - s(1,2) \quad \text{(PY)} \tag{4.6.17}$$

While this interpretation is certainly correct it is important not to misunderstand its meaning. In particular, it does not imply that the PY approximation represents a partial summation of the diagrammatic expansion of $b(r)$. On the contrary, the diagrammatic effect of (4.6.17) is to replace the bridge diagrams by star products of series diagrams.

The results just given make it possible to understand, at least for low densities, why the PY results for hard spheres, and more generally for potentials with a strongly repulsive core, are superior to those obtained from the HNC equation. The coefficient of the term of order ρ^n in the density expansion (4.6.4) of the pair distribution function of a homogeneous fluid is given by the sum of all diagrams in (4.6.3) that contain precisely n black circles. Thus $g_1(r)$ is represented by the single diagram

$g_1(r) =$ 

and $g_2(r)$ is the sum of five diagrams:

$g_2(r) =$ 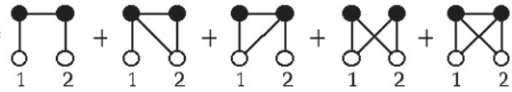

where all black circles are now 1-circles and the second and third diagrams in the expression for $g_2(r)$ are equal in value. The diagram representing $g_1(r)$ is

also the first-order diagram in the expansion of $s(r)$, showing that (4.6.15) and (4.6.16) are both exact to order ρ. At second order the HNC approximation is obtained by discarding the bridge diagram in the exact expression. Thus

$g_2(r) \approx$ 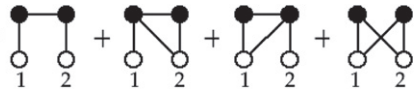 (HNC)

If the bridge function is written as a power series in density:

$$b(r) = b^{(2)}(r)\rho^2 + b^{(3)}(r)\rho^3 + \cdots \tag{4.6.18}$$

then in the PY approximation the coefficient of the second-order term is

$$b^{(2)}(r) = -\frac{1}{2}\left[g_1(r)\right]^2 \tag{4.6.19}$$

or, diagrammatically:

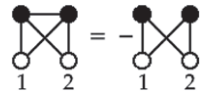

where the factor $\frac{1}{2}$ is taken care of by the symmetry number of the product diagram. The contributions from the bridge and product diagrams in the exact expression for $g_2(r)$ therefore cancel each other to give

$g_2(r) \approx$ 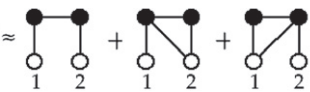 (PY)

The same result follows directly from (4.6.16).

The relative merits of the two approximations can be tested numerically in the case of hard spheres, since analytical expressions are available[23b] for the different contributions to the exact result for $g_2(r)$. The results are shown in Figure 4.7, from which it is clear that the cancellation on which the PY approximation for $g_2(r)$ rests is nearly complete; it becomes exact for $r \geq \sqrt{3}d$. Discarding both the bridge and product diagrams is therefore an improvement on omission of the bridge diagram alone. Complete cancellation would be achieved if the f-bond linking the two black circles of the bridge diagram were set equal to -1. This is an approximation that is clearly most appropriate for hard spheres, for which $f(r)$ takes only the values -1 or zero depending on whether r is less than or greater than d; as the potential softens it becomes more difficult to justify. Numerically the effect is small because the value of the bridge diagram is largely determined by the contribution from regions in which the coordinates associated with the black circles are separated by distances shorter than d. Similar considerations apply at higher densities.[28]

The derivation of the Debye–Hückel expression for the radial distribution function of a system of charged particles provides a simple but useful example

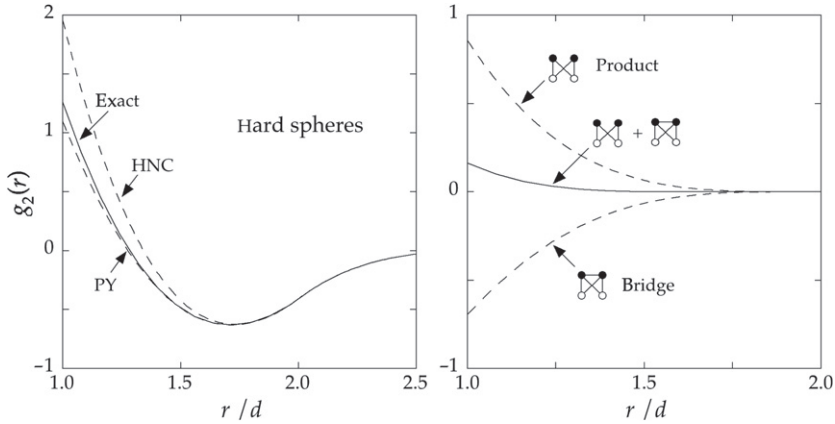

FIGURE 4.7 Left-hand panel: The coefficient $g_2(r)$ in the density expansion of the pair distribution function of the homogeneous hard-sphere fluid; the full curve gives the exact result, and the dashed curves show the results obtained from the HNC and PY approximations. Right-hand panel: The dashed curves are the contributions to the exact result for $g_2(r)$ from the product diagram (above) and the bridge diagram (below), and the full curve is the sum of the two.

of the application of diagrammatic techniques to the calculation of pair functions. Consider a homogeneous, one-component plasma of point charges q, immersed in a neutralising, uniform background of opposite charge, for which the pair potential[29] is

$$v(r) = q^2/r \tag{4.6.20}$$

Use of (4.6.20) in expansions of the pair functions leads to divergent integrals but convergent results can be obtained if entire classes of diagrams are summed. The most strongly divergent integrals in the expansion of $\omega(1,2)$ are those associated with the most weakly connected diagrams, namely the chain diagrams. If the chain diagrams are summed to all orders in ρ, but all other diagrams are ignored, the result is an approximation for $\omega(1,2)$ of the form

$\omega(1,2) \approx$ [all chain diagrams consisting of two terminal white1-circles labelled 1 and 2, one or more black ρ-circles and f-bonds]

$=$ 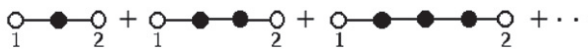 $+ \cdots$ (4.6.21)

By analogy with (3.5.10) and (4.6.1), $\omega(1,2)$ is given by

$$\omega(1,2) = \rho \int f(1,3)[f(3,2) + \omega(3,2)]\,\mathrm{d}3 \tag{4.6.22}$$

On taking Fourier transforms (4.6.22) becomes

$$\hat{\omega}(k) = \frac{\rho[\hat{f}(k)]^2}{1 - \rho\hat{f}(k)} \tag{4.6.23}$$

with

$$\rho \hat{f}(k) = \rho \int \exp(-i\mathbf{k}\cdot\mathbf{r}) f(r)\, \mathrm{d}\mathbf{r}$$
$$\approx -\beta\rho q^2 \int \frac{\exp(-i\mathbf{k}\cdot\mathbf{r})}{r} \mathrm{d}\mathbf{r} = -\frac{k_\mathrm{D}^2}{k^2} \tag{4.6.24}$$

where

$$k_\mathrm{D} = (4\pi\beta\rho q^2)^{1/2} \tag{4.6.25}$$

is the Debye wavenumber. We now substitute for $\rho\hat{f}(k)$ in (4.6.23) and find that

$$\rho[\hat{\omega}(k) - \beta\hat{v}(k)] = \frac{k_\mathrm{D}^2}{k_\mathrm{D}^2 + k^2} \tag{4.6.26}$$

or

$$\omega(r) - \beta v(r) = -\beta\psi(r) = -\frac{\beta q^2}{r}\exp(-k_\mathrm{D} r) \tag{4.6.27}$$

We see that summing the chain diagrams leads to a potential of mean force or 'renormalised' potential equal to $v(r)\exp(-k_\mathrm{D}r)$. This damping of the Coulomb potential by the factor $\exp(-k_\mathrm{D}r)$ is familiar from elementary Debye–Hückel theory and corresponds physically to the effects of screening. It follows from (4.6.5) that the corresponding approximation for the radial distribution function is

$$g(r) = \exp\left(-\frac{\beta q^2}{r}\exp(-k_\mathrm{D}r)\right) \tag{4.6.28}$$

Equation (4.6.28) is more familiar in its linearised form, valid for $k_\mathrm{D}r \gg 1$, i.e.

$$g(r) \approx 1 - \frac{\beta q^2}{r}\exp(-k_\mathrm{D}r) \tag{4.6.29}$$

This result could have been obtained more directly by replacing $c(r)$ by $-\beta v(r)$ in (4.6.1). A serious weakness of the linearised approximation is the fact that it allows $g(r)$ to become negative at small r; this failing is rectified in the non-linear version (4.6.28).

The pair functions discussed in this section, together with their definitions, are summarised in Table 4.1.

4.7 EXTENSIONS OF INTEGRAL EQUATIONS

We saw in the previous section that the development of an accurate integral equation for $g(r)$ can be reduced to the problem of devising a satisfactory approximation for the bridge function $b(r)$. The HNC approximations consists in setting $b(r) = 0$. Hence the integral equations to which some other

TABLE 4.1 Selected pair functions and their definitions.

Function	Symbol	Definition	
Pair distribution function	$g(r)$	(2.5.15)	
Pair correlation function	$h(r)$	$g(r) - 1$	(4.6.2)[a]
Direct correlation function	$c(r)$	(3.5.2), (3.5.10)	(3.8.7)[a]
Cavity distribution function	$y(r)$	$\exp[\beta v(r)]\, g(r)$	(4.6.3)[a]
Potential of mean force	$\psi(r)$	$-k_B T \ln g(r)$	
[Unnamed]	$\omega(r)$	$\ln y(r)$	(4.6.9)[a]
Indirect correlation function	$s(r)$	$h(r) - c(r)$	(4.6.11)[a]
Bridge function	$b(r)$	$\omega(r) - s(r)$	(4.6.12)[a]

[a] *Diagrammatic expansion.*

approximation, $b(r) \approx b_0(r)$ say, gives rise can be regarded as a modified HNC equation in which the exact relation (4.6.13) is replaced by

$$\ln g(r) = -\beta[v(r) - k_B T b_0(r)] + h(r) - c(r) \tag{4.7.1}$$

The task of solving the modified equation is therefore equivalent to finding the solution to the HNC equation for an effective potential $v_{\text{eff}}(r)$ defined as

$$v_{\text{eff}}(r) = v(r) - k_B T b_0(r) \tag{4.7.2}$$

It is possible to improve the HNC approximation systematically by including successively higher-order terms in the series expansion of the bridge function, but the calculations are computationally demanding and the slow convergence of the series means that in general only modest improvement is achieved.[30]

The true bridge function for a given system can be calculated from (4.6.14) if $c(r)$, $h(r)$ and $y(r)$ are known. A conventional simulation provides values of $h(r)$ at separations where $g(r)$ is non-zero, from which $c(r)$ for all r can be obtained via the Ornstein–Zernike relation; in this range of r the calculation of $y(r)$ from $h(r)$ is a trivial task. To determine $b(r)$ at smaller separations, where $h(r) \approx -1$, an independent calculation of $y(r)$ is required. This can be achieved by simulation of the mixed system, described in the previous section, in which the particles labelled 1 and 2 do not interact with each other. The calculation is straightforward in principle, but the very rapid rise in $y(r)$ as $r \to 0$ means that special techniques are needed to ensure that the full range of r is adequately sampled.[24,31]

Figure 4.8 shows the bridge function derived from Monte Carlo calculations for the Lennard-Jones fluid in a thermodynamic state not far from the triple point and compares the results with those given by the PY approximation (4.6.17). In the example illustrated, the bridge function makes a contribution to the effective potential (4.7.2) that is both short ranged and predominantly repulsive, but the

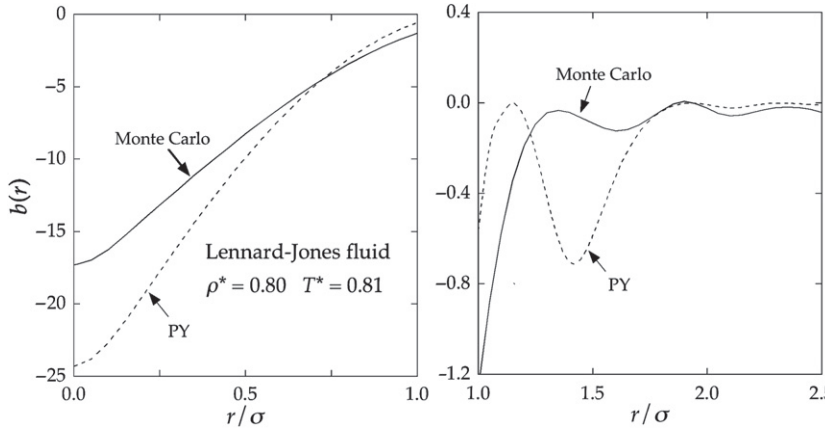

FIGURE 4.8 Bridge function of the Lennard-Jones fluid obtained by Monte Carlo calculations for $r < \sigma$ (left) and $r > \sigma$ (right). The PY results are those given by (4.6.17). After Llano–Restrepo and Chapman.[24]

same is true for the Lennard-Jones fluid at other thermodynamic states and for other model fluids. The PY approximation is poor at small values of r, but in that region the pair potential is so strongly repulsive that errors in the effective potential are unimportant for many purposes. So far as the calculation of thermodynamic properties is concerned, the most serious deficiencies in the PY approximation occur in the region of the main peak in $g(r)$.

Alternatives to the PY approximation have been proposed[32] that resemble (4.6.17) insofar as $b(r)$ is written as a function of $s(r)$. These approximations give results for the hard-sphere fluid that improve on those obtained from the PY equation and they have also been applied, though with generally less success, to systems having an attractive term in the potential. There is no reason to suppose, however, that the functional relationship between $b(r)$ and $s(r)$ is the same for all potentials, or even for different thermodynamic states of a given system.[24,33] To improve on the PY or PY-like approximations it seems necessary to make the assumed form of $b(r)$ explicitly dependent on $v(r)$. The soft-core MSA (SMSA) discussed in Section 4.5 provides an example of how this can be done. From the SMSA expression for $g(r)$ given by (4.5.9) it follows that

$$y(r) \equiv \exp\left[\beta v(r)\right] g(r) = \exp\left[\beta v_1(r)\right]\left[1 + s(r) - \beta v_1(r)\right] \tag{4.7.3}$$

where $v_1(r)$ is the tail in the potential. Comparison with (4.6.13) shows that this is equivalent to replacing the bridge function by

$$b(r) \approx \ln[1 + s^*(r)] - s^*(r) \quad \text{(SMSA)} \tag{4.7.4}$$

where

$$s^*(r) = s(r) - \beta v_1(r) \tag{4.7.5}$$

Equation (4.7.4) is identical to its PY counterpart (4.6.17) but with $s(r)$ replaced by $s^*(r)$. The result, as we have seen, is a marked improvement relative to the PY approximation in the case of the Lennard-Jones fluid.

We showed in Section 4.3 that the HNC approximation can be derived by minimising the grand potential functional obtained from a functional Taylor expansion of the intrinsic free energy truncated at second order. The question therefore arises as to whether any significant improvement is obtained when the third-order term is included.[5] Equation (4.3.10) again provides the starting point of the calculation, but $c^{(2)}(\mathbf{r},\mathbf{r}';\lambda)$ is now replaced, not by $c_0^{(2)}(\mathbf{r},\mathbf{r}')$, but by

$$\begin{aligned} c^{(2)}(\mathbf{r},\mathbf{r}';\lambda) &\approx c_0^{(2)}(\mathbf{r},\mathbf{r}') + \lambda \int \Delta\rho^{(1)}(\mathbf{r}'') \frac{\delta c_0^{(2)}(\mathbf{r},\mathbf{r}')}{\delta\rho^{(1)}(\mathbf{r}'')}\, \mathrm{d}\mathbf{r}'' \\ &= c_0^{(2)}(\mathbf{r},\mathbf{r}') + \lambda \int \Delta\rho^{(1)}(\mathbf{r}'') c_0^{(3)}(\mathbf{r},\mathbf{r}',\mathbf{r}'')\, \mathrm{d}\mathbf{r}'' \end{aligned} \tag{4.7.6}$$

where $c_0^{(3)}(\mathbf{r},\mathbf{r}',\mathbf{r}'')$ is the three-particle direct correlation function of the reference fluid. The effect is to add to the functional (4.3.14) the term

$$-\frac{1}{6}k_{\mathrm{B}}T \iiint \Delta\rho^{(1)}(\mathbf{r})\Delta\rho^{(1)}(\mathbf{r}')\Delta\rho^{(1)}(\mathbf{r}'')c_0^{(3)}(\mathbf{r},\mathbf{r}',\mathbf{r}'')\, \mathrm{d}\mathbf{r}\, \mathrm{d}\mathbf{r}'\, \mathrm{d}\mathbf{r}''$$

If we now follow the steps that previously led to the HNC approximation (4.3.19), we obtain an expression for the pair distribution function of a uniform fluid having the form (4.7.1), with

$$b_0(r) = 12\rho^2 \iint c^{(3)}(\mathbf{r}-\mathbf{r}',\mathbf{r}-\mathbf{r}'')h(r')h(r'')\, \mathrm{d}\mathbf{r}'\, \mathrm{d}\mathbf{r}'' \tag{4.7.7}$$

Solution of the integral equation for $g(r)$ requires some further approximation[5] to be made for the triplet function $c^{(3)}$. Equation (4.7.7) is equivalent to the lengthier expression in terms of $g^{(3)}$ obtained from an expansion of $c^{(1)}(\mathbf{r})$ taken to second order, the so-called HNC2 approximation.[34]

Results based on (4.7.7) show a clear improvement over the HNC approximation for a number of model fluids but the method is computationally demanding. The HNC equation can more easily and successfully be extended by identifying $b_0(r)$ with the bridge function of a suitable reference system, a step that leads to the 'reference' HNC (RHNC) approximation.[35] The obvious choice of reference system is a fluid of hard spheres, since this is the only potential model for which the bridge function is known with sufficient accuracy over the full range of state conditions.[36] Equation (4.7.1) then represents a one-parameter theory in which the only unknown quantity is the hard-sphere diameter d. It was originally argued that the bridge function was likely to be highly insensitive to details of the potential and that its representation by a hard-sphere function should therefore be a good approximation. Although it is now recognised that the bridge function does not have a genuinely 'universal' character,[37] this approach

TABLE 4.2 Thermodynamic properties of the Lennard-Jones fluid: comparison between molecular dynamics results (MD) and calculations based on the RHNC approximation. After Lado et al.[35c]

		$\beta P/\rho$		$\beta U^{ex}/N$	
ρ^*	T^*	MD	RHNC	MD	RHNC
0.85	0.719	0.36	0.424	−6.12	−6.116
0.85	2.889	4.36	4.364	−4.25	−4.240
0.75	1.071	0.89	0.852	−5.17	−5.166
0.65	1.036	−0.11	−0.155	−4.52	−4.522
0.65	2.557	2.14	2.136	−3.78	−3.786
0.45	1.552	0.57	0.552	−2.98	−2.982
0.45	2.935	1.38	1.377	−2.60	−2.608
0.40	1.424	0.38	0.382	−2.73	−2.728

has been applied successfully in calculations for a variety of different systems. The overall agreement with the results of simulations is very good, as illustrated by the results for thermodynamic properties of the Lennard-Jones fluid given in Table 4.2; the errors in the corresponding pair distribution functions are barely discernible, even under conditions close to the triple point. In the work on which Table 4.2 is based, the hard-sphere diameter was chosen in such a way as to minimise an approximate free energy functional. So far as internal consistency of the theory is concerned, use of this procedure gives the RHNC approximation a status comparable with that of the HNC equation. The method has also been applied to mixtures of Lennard-Jones fluids, again with very good results.[35e]

A number of attempts have been made to combine different closure relations in hybrid schemes that ensure a degree of thermodynamic consistency. For example, whereas the HNC approximation is correct at large separations, the PY approximation, being much superior for strongly repulsive potentials, is presumably more accurate at short distances. It is therefore plausible to mix the two closures in such a way[38] that the function $y(r)$ in (4.6.14) reduces to its PY value as $r \to 0$ and to its HNC value as $r \to \infty$. The parameter that determines the proportions in which the two approximations are mixed at intermediate values of r can then be chosen to force consistency between the compressibility and virial equations of state. The method works well for systems of particles interacting through purely repulsive potentials, but breaks down for the Lennard-Jones potential for which, at low temperatures, it is impossible to find a value of the mixing parameter that provides thermodynamic consistency. Where successful, the method relies heavily on the fact that the HNC and PY approximations in some sense bracket the exact solution for the system of interest. The difficulty in the case of the Lennard-Jones fluid lies in the fact

that the PY approximation is poor at low temperatures. The problem can be overcome[39] by interpolating instead between the HNC approximation and the soft-core MSA, an approach – called the HMSA – that yields results comparable in quality with those obtained by the RHNC approximation.

A more ambitious method of building thermodynamic consistency into an integral equation theory is to write the direct correlation function in a form that can be adjusted so as to satisfy some consistency criterion. This is the basis of the self-consistent Ornstein–Zernike approximation or SCOZA developed by Stell and coworkers[40] for application to potentials consisting of a hard core and a tail, $v_1(r)$ say, as in (4.5.1). Since $g(r)$ vanishes inside the hard core, closure of the Ornstein–Zernike is achieved by making some approximation for $c(r)$ in the range $r > d$; this is typically of the form

$$c(r) = c_d(r) - \alpha(\rho, T)v_1(r), \quad r > d \tag{4.7.8}$$

where $c_d(r)$ is the direct correlation function of the hard-sphere fluid. The quantity $\alpha(\rho, T)$, which plays the role of an effective, density-dependent, inverse temperature, can then be chosen in such a way as to enforce consistency between the compressibility and energy routes to the equation of state. Equation (4.7.8) resembles certain other closure relations insofar as the range of $c(r)$ is the same as that of the pair potential, but in contrast, say, to the MSA, its amplitude is now density-dependent. If the compressibility and internal energy are to be consistent with each other, they must come from the same free energy, and hence must satisfy the relation[41]

$$-\frac{\partial \hat{c}(k=0)}{\partial \beta} = \frac{\partial^2 u}{\partial \rho^2} \tag{4.7.9}$$

thereby providing a partial differential equation for $\alpha(\rho, T)$; here $u \equiv U^{\text{ex}}/V$ while $\hat{c}(k=0)$ is related to the compressibility by (3.5.15).

Most of the published calculations based on the SCOZA are concerned with the hard-core Yukawa model (1.2.2), a system for which the analytical solution to the MSA is known.[42] A major simplification of the problem is then possible. If $c_d(r)$ for $r > d$ is represented by a second Yukawa term, $\hat{c}(k=0)$ can be related analytically to u and (4.7.9) becomes a partial differential equation for the variable $u(\rho, T)$, which can be solved numerically; the two free parameters in the second Yukawa term are chosen so as to reproduce the Carnahan–Starling equation of state in the limit $T \to \infty$. The same simplification applies when the long-range contribution to the potential is represented by a linear combination of Yukawa terms, a strategy that makes it possible to mimic a variety of pair potentials of physical interest.[43] For other choices of $v_1(r)$, such as that provided by the square-well potential,[43,44] a fully numerical solution is required, thereby substantially increasing the computational effort involved. The SCOZA gives good results for the structure and thermodynamics of the Yukawa and square-well fluids over a range of state conditions and choices of the Yukawa

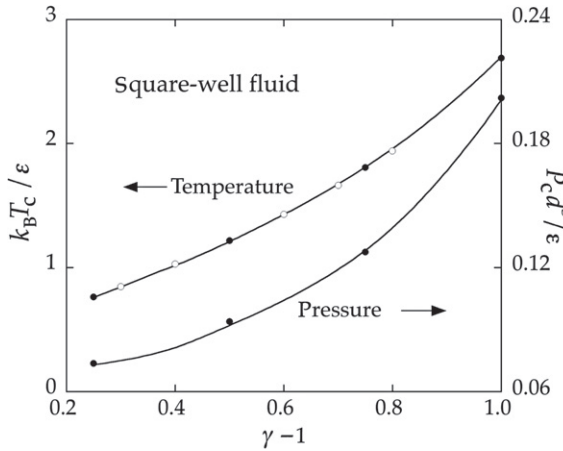

FIGURE 4.9 Critical temperature and critical pressure of the square-well fluid as a function of the well width ($\gamma - 1$) in units of d. The curves are calculated from the SCOZA[44a]; the symbols show the results of Monte Carlo simulations.[45]

inverse-range parameter γ or the well-width parameter in the square-well potential (see Figure 1.2), but its chief merit is the fact that it remains accurate in the critical region, where the performance of other integral equation theories is mostly poor. The success of the SCOZA in the case of the square-well fluid is illustrated in Figure 4.9, which shows the behaviour of the reduced critical temperature and critical pressure as functions of γ. Agreement with the results of Monte Carlo calculations is excellent for both properties. There are, however, some differences between theory and simulation in the results for the critical density; these discrepancies increase as the range of the attractive interaction is reduced, a trend that is also apparent in calculations for the Yukawa fluid.[46]

4.8 ASYMPTOTIC DECAY OF THE PAIR CORRELATION FUNCTION

Results from simulations, integral equation approximations and radiation scattering experiments invariably show that in the liquid range the pair correlation function decays to zero in the damped, oscillatory manner exemplified in Figures 2.3 and 3.2. At low densities, by contrast, it decays monotonically. The oscillatory decay is associated with packing-induced layering of neighbours around a central particle, while at low density the result in (2.6.10) implies that the decay of $h(r)$ is governed by the behaviour of the pair potential at large r. Working on the basis of a one-dimensional model, Fisher and Widom[47] predicted that at least for short-range potentials there should be

a sharp cross-over from monotonic to oscillatory decay along a locus of points in the density–temperature plane, now termed the Fisher–Widom line.

We take as a starting point the diagrammatic expansion of the direct correlation function in (3.8.7) and the discussion that follows, which tell us that $c(r)$ behaves as $-\beta v(r)$ as $r \to \infty$. Consider first the case of short-range potentials,[48] either of finite range, vanishing beyond some cut-off value, or decaying exponentially at large r. The Fourier transform $\hat{c}(k)$ of such potentials can be expanded in even powers of k:

$$\hat{c}(k) = c_0 + c_2 k^2 + c_4 k^4 + \mathcal{O}(k^6) \tag{4.8.1}$$

The Ornstein–Zernike relation (3.5.13) expresses $\hat{h}(k)$ in terms of $\hat{c}(k)$ and an inverse Fourier transform yields an expression for $h(r)$ that can be written in two equivalent forms, either

$$rh(r) = \frac{1}{4\pi^2 i} \int_{-\infty}^{\infty} \exp(ikr) \frac{\hat{c}(k)}{1 - \rho\hat{c}(k)} k \, \mathrm{d}k \tag{4.8.2}$$

or

$$rh(r) = \frac{1}{2\pi^2} \operatorname{Im} \int_{0}^{\infty} \exp(ikr) \frac{\hat{c}(k)}{1 - \rho\hat{c}(k)} k \, \mathrm{d}k \tag{4.8.3}$$

If $\hat{c}(k)$ is a known function, the integrals on the right-hand side of these equations can be evaluated by contour integration in the plane of complex wavenumbers, $k = k_1 + ik_2$, pictured schematically in Figure 4.10. The poles of the integrand correspond to zeros of the denominator, given by the complex solutions of the equation

$$1 - \rho\hat{c}(k) = 0 \tag{4.8.4}$$

To calculate the integral in (4.8.2) the contour must be closed by an infinite semi-circle in the upper half-plane. The value of the integral is the sum of the

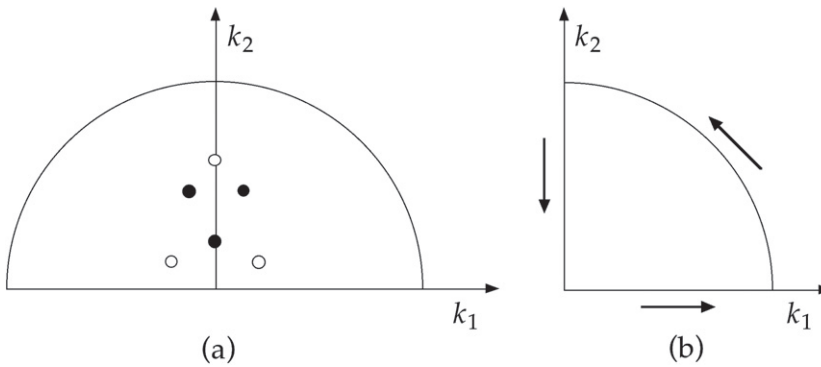

FIGURE 4.10 The complex wavenumber plane. (a) The open and closed circles show two possible distributions of the poles of $\hat{h}(k)$ lying closest to the real axis; see text for details. (b) Contour used in the evaluation of the integral in (4.8.3).

residues at the poles, and a pair of equations that together determine the real and imaginary parts of the poles is obtained by taking the real and imaginary parts of (4.8.4):

$$\begin{aligned} 4\pi\rho \int_0^\infty c(r) \frac{\sinh(k_2 r)}{k_2 r} \cos(k_1 r) r^2 \, \mathrm{d}r &= 1 \\ 4\pi\rho \int_0^\infty c(r) \cosh(k_2 r) \frac{\sin(k_1 r)}{k_1 r} r^2 \, \mathrm{d}r &= 1 \end{aligned} \tag{4.8.5}$$

If R_n is the residue of $\hat{c}(k)/[1 - \rho\hat{c}(k)]$ at the nth pole, $k = k^{(n)}$, the integral in (4.8.2) reduces to

$$rh(r) = \frac{1}{2\pi} \sum_n R_n \exp\left(k^{(n)} r\right) = \frac{1}{2\pi} \sum_n R_n \exp\left(-ik_2^{(n)} r\right) \exp\left(ik_1^{(n)} r\right) \tag{4.8.6}$$

The poles may lie on the imaginary axis, $k_1^{(n)} = 0$, or may form a conjugate pair, $k^{(n)} = \pm k_1^{(n)} + ik_2^{(n)}$. In the first case the contribution to the decay of $rh(r)$ from the single pole is purely exponential; in the second case there is a damped, oscillatory contribution from the conjugate pair. There could in principle be an infinite number of such terms but the presence of the exponential factors in (4.8.6) ensures that asymptotically the dominant contribution will come from the pole or poles nearest the real axis. Two scenarios are therefore possible. If the nearest pole is purely imaginary, corresponding to the black circles in Figure 4.10, then

$$\lim_{r\to\infty} h(r) = \frac{A}{r} \exp(-k_2 r) \tag{4.8.7}$$

where the amplitude $A = R/2\pi$, with R being the residue at the pole. If all poles are simple, the residue theorem implies that

$$A = \frac{-ik_2}{2\pi\rho^2 \hat{c}'(ik_2)} \tag{4.8.8}$$

where the prime denotes a derivative with respect to the argument; then differentiation of the Fourier transform of $c(r)$ shows that for $k = ik_2$:

$$\hat{c}'(ik_2) = \frac{4\pi}{ik_2} \int_0^\infty c(r) \left(\cosh(k_2 r) - \frac{\sinh(k_2 r)}{k_2 r} \right) r^2 \, \mathrm{d}r \tag{4.8.9}$$

Alternatively, if the poles closest to the real axis form a conjugate pair, corresponding to the white circles in the figure, the asymptotic behaviour is oscillatory:

$$\lim_{r\to\infty} h(r) = \frac{2|A|}{r} \exp(-k_2 r) \cos(k_1 r - \theta) \tag{4.8.10}$$

where the amplitude $|A|$ and phase angle θ are related by

$$|A| \exp(-i\theta) = -\frac{k_1 + ik_2}{2\pi\rho^2 \hat{c}'(k_1 + ik_2)} \tag{4.8.11}$$

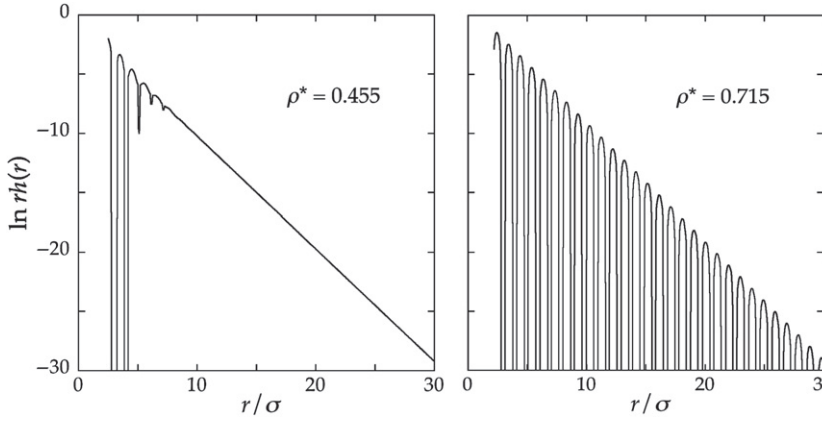

FIGURE 4.11 Asymptotic behaviour of the function $\ln rh(r)$ predicted by the pole analysis described in the text for the truncated Lennard-Jones fluid at $T^* = 1.2$ and two densities. From R.J.F. Leote de Carvalho et al., 'The decay of the pair correlation function in simple fluids: long- versus short-ranged potentials', *J. Phys. Condens. Matter* **6**, 9275–9294 (1994).

Calculations that use as input the direct correlation functions derived from integral equation approximations show that the relative positions of the lowest-lying imaginary and complex conjugate poles change as the density increases along an isotherm.[48] At low densities, the purely imaginary pole lies below the conjugate pair and $h(r)$ is found to decay monotonically; at high densities the situation is reversed, leading to an oscillatory decay. The cross-over in relative positions of the poles defines a point on the Fisher–Widom line. The curves of the function $\ln rh(r)$ plotted in Figure 4.11 illustrate the striking difference in asymptotic behaviour at densities on different sides of the Fisher–Widom line in the case of the Lennard-Jones potential truncated[49] at $r = 2.5\sigma$. The results shown are the contributions to the expansion (4.8.6) from the poles pictured in Figure 4.10, calculated from input provided by numerical solution of the HMSA equation of Section 4.9, which is known to be very accurate. Beyond $r \approx 2\sigma$ they are indistinguishable on the scale of the figure from the results derived directly from the HMSA values of $h(r)$. Some oscillations are seen at intermediate values of r even at low density, but these rapidly merge into an exponential decay; at high density the oscillations are exponentially damped but persisting. By repeating the calculations for a large number of points in the density–temperature plane it possible to map out the Fisher–Widom line for the potential, with the results shown in Figure 4.12. The line intersects the liquid–vapour coexistence curve on the liquid side at $T/T_c \approx 0.9$ and $\rho/\rho_c \approx 1.8$, numbers that are very close to those obtained in similar calculations for the square-well fluid.

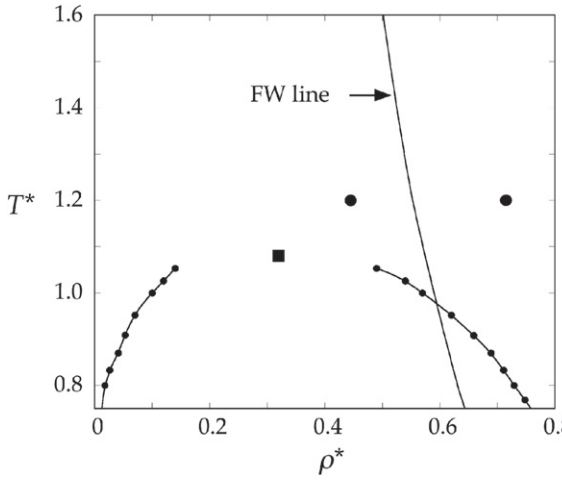

FIGURE 4.12 The Fisher–Widom line for the truncated Lennard-Jones fluid calculated from the HMSA. The small black circles show the results of Monte Carlo calculations[50] of the liquid–vapour coexistence curve, with lines drawn as a guide to the eye. The square is the Monte Carlo estimate of the critical point and the large black circles mark the state points for which the results shown in Figure 4.11 were calculated. From R.J.F. Leote de Carvalho et al., 'The decay of the pair correlation function in simple fluids: long- versus short-ranged potentials', *J. Phys. Condens. Matter* **6**, 9275–9294 (1994).© *IOP Publishing 1994. Reproduced by permission of IOP Publishing. All rights reserved.*

The asymptotic analysis is more complicated for potentials that decay as a power law, as is the case for dispersion forces, where the dominant interaction at large r is $v(r) \approx -a_6/r^6$, with a Fourier transform given by

$$\hat{v}(k) = -\frac{\pi^2 a_6}{12} k^3 \tag{4.8.12}$$

The dependence on k^3 means that the $\hat{c}(k)$ can no longer be expanded purely in terms of even powers of k. Instead we can write

$$\hat{c}(k) = \hat{c}^{\mathrm{sr}}(k) + ak^3 \tag{4.8.13}$$

where the short-range part $\hat{c}^{\mathrm{sr}}(k)$ can be expanded in the manner of (4.8.1) and a is the coefficient (apart from the negative sign) of k^3 in (4.8.12). In this case the function $rh(r)$ is evaluated by contour integration of (4.8.3) with the contour taken around the upper-right quadrant of the complex plane (see Figure 4.10). The contribution from the circular part vanishes. Hence, from the residue theorem, the integral is given by

$$rh(r) = \frac{1}{2\pi^2}\mathrm{Im}\left(2\pi i \sum_n \exp\left(ik^{(n)}r\right)R_n + \int_0^\infty ik_2 \exp\left(-k_2 r\right)\frac{\hat{c}(ik_2)}{1-\rho\hat{c}(ik_2)}\,\mathrm{d}(ik_2)\right) \tag{4.8.14}$$

where R_n is the residue at a pole $k^{(n)}$ in the upper-right quadrant. The poles are again the roots of (4.8.4), which now has the form

$$1 - \rho\left[\hat{c}^{\mathrm{sr}}(k) + ak^3\right] = 0 \tag{4.8.15}$$

The presence of the term in k^3 means that there are no purely imaginary solutions to this equation and hence no poles on the imaginary axis. In fact, since $\hat{c}^{\mathrm{sr}}(k)$ is a real function, the imaginary part of (4.8.15) implies that $k_2 = 0$. It is precisely the absence of poles on the imaginary axis that allows the use of the contour shown in Figure 4.10.

The final task is to determine the long-range behaviour of the integral, $I(r)$, on the right-hand side of (4.8.14), which can be rewritten in the form

$$I(r) = \frac{1}{2\pi^2\rho}\mathrm{Im}\int_0^\infty k_2 \exp(-k_2 r)\left(1 - \frac{1}{1 - \rho\hat{c}(ik_2)}\right)\mathrm{d}k_2 \tag{4.8.16}$$

The first term in large brackets leads to a real integral; what remains is

$$I(r) = -\frac{1}{2\pi^2\rho}\mathrm{Im}\int_0^\infty k_2 \exp(-k_2 r)\frac{1}{1 - \rho\left[\hat{c}^{\mathrm{sr}}(ik_2) - iak_2^3\right]}\mathrm{d}k_2 \tag{4.8.17}$$

The presence of the exponential factor means that the integral is dominated by the contribution from small k_2. Use of the expansion (4.8.1) for $\hat{c}^{\mathrm{sr}}(k)$ and Taylor expansion of the integrand to order k_2^4 leads, after taking the imaginary part, to

$$\begin{aligned} I(r) &= \frac{a}{2\pi^2}\frac{1}{\left[1 - \rho\hat{c}^{\mathrm{sr}}(k=0)\right]^2}\int_0^\infty \exp(-k_2 r)\left[k_2^4 + \mathcal{O}(k_2^6)\right]\mathrm{d}k_2 \\ &= \beta a_6 S(0)^2\frac{1}{r^5} + \mathcal{O}(r^{-7}) \end{aligned} \tag{4.8.18}$$

where $S(0)$ is the long-wavelength limit of the static structure factor and (3.6.10), (4.8.12) and (4.8.13) have been used. Thus, from (4.8.14), and by analogy with (4.8.10), we find that

$$h(r) = [S(0)]^2\frac{\beta a_6}{r^6} + \sum_n |A_n| \exp\left(-k_2^{(n)} r\right)\cos\left(k_1^{(n)} r - \theta_n\right) \tag{4.8.19}$$

where the second term is the contribution from all poles within the upper-right quadrant of the complex plane. The absence of the factor 2 in front of the sum compared with (4.8.10) comes from the fact that the conjugate poles in the upper-left quadrant make no contribution. The conclusion, therefore, is that at large r, $h(r)$ behaves in the same manner as $c(r)$ but with a prefactor which is small in dense, weakly compressible liquids. The same result had been arrived at earlier and via a different route by Enderby et al.[51]

The picture of the asymptotic behaviour of $h(r)$ presented by (4.8.19) is that of oscillations which eventually merge into a power law decay. The effect of increasing density at constant temperature is simply to increase the value of r at which the oscillations disappear. Hence there is no sharp cross-over between different regimes of the type found for short-range potentials, for which there is a pure exponential contribution to the decay. Efforts have been made[52] to redefine the Fisher–Widom line to cater for such a situation, based on a more detailed study of the pole structure for potentials that behave as r^{-6}. This has revealed that although there can be no purely imaginary pole, there is a 'pseudo-exponential' pole that lies off the imaginary axis but very close to it, the contribution from which substantially modifies the asymptotic decay.

The extension of the asymptotic analysis to binary mixtures is straightforward but it leads to some surprising results.[48a] The k-space representation of the Ornstein–Zernike relations (3.6.12) is

$$\hat{h}_{\nu\mu}(k) = \hat{c}_{\nu\mu}(k) + \sum_{\lambda} \rho_\lambda \hat{c}_{\nu\lambda}(k)\hat{h}_{\lambda\mu}(k) \tag{4.8.20}$$

where $\rho_\lambda = x_\lambda \rho$. These coupled equations can be solved for $\hat{h}_{\nu\mu}(k)$ in the form of ratios of k-space functions, a key feature of which is the fact that the denominator is the same for all ν, μ. The poles of $\hat{h}_{\nu\mu}(k)$ are given by the zeros of this common denominator and are therefore the same for all pairs. The functions $h_{\nu\mu}(r)$ can again be calculated by contour integration with a result given by a generalisation of (4.8.6);

$$rh_{\nu\mu}(r) = \frac{1}{2\pi} \sum_{n} R_n^{\nu\mu} \exp\left(ik^{(n)}r\right) \tag{4.8.21}$$

which implies that asymptotically all pair correlation functions decay with the same characteristic length, $2\pi/k_2$, and the same oscillatory period, $2\pi/k_1$, where k_1 and k_2 are the real and imaginary parts of the pole or poles nearest to the real axis, conclusions that are somewhat counter–intuitive. The amplitude and phase of oscillation will, however, be different. Explicit calculations for highly size-asymmetric, binary mixtures of hard spheres show that the period of oscillation is close to the diameter of the larger species.

The decay of the density profile at a planar, fluid–fluid or wall–fluid interface can also be analysed along the same lines as those we have described. Calculation of the asymptotic behaviour close to the critical point or in ionic liquids[53] introduces new problems, discussion of which is deferred until Sections 5.7 and 10.3, respectively.

REFERENCES

[1] Kirkwood, J.G., *J. Chem. Phys.* **3**, 300 (1935).

[2] Born, M. and Green M.S., 'A General Kinetic Theory of Liquids'. Cambridge University Press, Cambridge, 1949.

[3] Levesque, D., *Physica* **32**, 1985 (1966).
[4] Ichimaru, S., *Phys. Rev. A* **2**, 494 (1970).
[5] Barrat, J.L., Hansen, J.P. and Pastore, G., *Mol. Phys*. **63**, 747 (1988).
[6] (a) Percus, J.K., *Phys. Rev. Lett*. **8**, 462 (1962).
(b) Percus, J.K., *In* 'The Equilibrium Theory of Classical Fluids' (H.L. Frisch and J.L. Lebowitz, eds). W.A. Benjamin, New York, 1964.
[7] The HNC approximation was developed independently by several workers. For some historical background, see Rowlinson, J.S., *Rep. Prog. Phys*. **28**, 169 (1965).
[8] (a) Gillan, M.J, *Mol. Phys*. **38**, 1781 (1979). (b) Labik, S., Malijevski, A. and Vonka, P., *Mol. Phys*. **56**, 709 (1985).
[9] The PY equation was originally derived in a very different way by Percus, J.K. and Yevick, G.J., *Phys. Rev*. **110**, 1 (1958).
[10] (a) Morita, T., *Prog. Theor. Phys*. **23**, 423, 829 (1960). (b) See also Schlijper, A.G., Telo da Gama, M.M. and Ferreira, P.G., *J. Chem. Phys*. **98**, 1534 (1993).
[11] (a) Thiele, E., *J. Chem. Phys*. **39**, 474 (1963). (b) Wertheim, M.S., *Phys. Rev. Lett*. **10**, 321 (1963). (c) Wertheim, M.S., *J. Math. Phys*. **5**, 643 (1964).
[12] Baxter, R.J. *Aust. J. Phys*. **21**, 563 (1968).
[13] (a) Lebowitz, J.L., *Phys. Rev*. **133**, A895 (1964). (b) Lebowitz, J.L. and Rowlinson, J.S., *J. Chem. Phys*. 41, 133 (1964).
[14] (a) Analytical expressions covering the range $x = 1$ to 5 are given by Smith, W.R. and Henderson, D., *Mol. Phys*. **19**, 411 (1970). (b) See also Chang, J. and Sandler, S.I., *Mol. Phys*. **81**, 735 (1994).
[15] (a) Verlet, L. and Weis, J.J., *Phys. Rev. A* **5**, 939 (1972). (b) The implementation of certain theories also requires a knowledge of the hard-sphere $y(r)$ inside the hard core, a parameterisation of which is given by Grundke, E.W. and Henderson, D., *Mol. Phys*. **24**, 269 (1972).
[16] Baxter, R.J., *J. Chem. Phys*. **49**, 2770 (1968).
[17] Hansen, J.P. and Verlet, L., *Phys. Rev*. **184**, 151 (1969).
[18] Chen, M., Henderson, D. and Barker, J.A., *Can. J. Phys*. **54**, 703 (1969).
[19] Smith, W.R., Henderson, D. and Tago Y., *J. Chem. Phys*. **67**, 5308 (1977).
[20] Madden, W.G., *J. Chem. Phys*. **75**, 1984 (1981).
[21] Madden, W.G. and Rice, S.A., *J. Chem. Phys*. **72**, 4208 (1980).
[22] This result was first derived by Mayer, J.E. and Montroll, E., *J. Chem. Phys*. **9**, 2 (1941). We recall from Section 3.7 that an irreducible diagram is one without articulation circles.
[23] (a) Kirkwood, J.G., *J. Chem. Phys*. **3**, 300 (1935). (b) Nijboer, B.R.A. and van Hove, L., *Phys. Rev*. **85**, 177 (1952).
[24] Llano-Restrepo, M. and Chapman, W.G., *J. Chem. Phys*. **97**, 2046 (1992).
[25] (a) In the case of hard spheres the limiting value as $r \to 0$ is equal to $\exp(\beta\mu^{\mathrm{ex}})$. See Hoover, W.G. and Poirier, J.C., *J. Chem. Phys*. **37**, 1041 (1962). (b) Widom, B., *J. Chem. Phys*. **39**, 2808 (1963).
[26] Hill, T.L., 'Introduction to Statistical Thermodynamics'. Addison-Wesley, Reading, 1960, p. 313.
[27] This transformation is achieved by a topological reduction based on Lemma 5 of Section 3.7.
[28] (a) Stell, G., *Physica* **29**, 517 (1963). (b) See also Attard, P., "Thermodynamics and Statistical Mechanics". Academic Press, London, 2002, Section 9.3.2.
[29] We use electrostatic units (esu).
[30] See, e.g. Perkyns, J.S., Dyer, K.M. and Pettitt, B.M., *J. Chem. Phys*. **116**, 9404 (2002).

[31] Torrie, G. and Patey, G.N., *Mol. Phys*. **34**, 1623 (1977).
[32] (a) For examples of this approach, see Caccamo, C., *Phys. Rep*. **274**, 1 (1996). (b) Bomont, J.M., *Adv. Chem. Phys*. **139**, 1 (2008).
[33] Fantoni, R. and Pastore, G. *J. Chem. Phys*. **120**, 10681 (2004).
[34] (a) Verlet, L., *Physica* **30**, 95 (1964). (b) Verlet, L., *Physica* **31**, 959 (1965).
[35] (a) Lado, F., *Phys. Rev. A* **8**, 2548 (1973). (b) Rosenfeld, Y. and Ashcroft, N.W., *Phys. Rev. A* **20**, 1208 (1979). (c) Lado, F., Foiles, S.M. and Ashcroft, N.W., *Phys. Rev. A* **28**, 2374 (1983). (d) Foiles, S.M., Ashcroft, N.W. and Reatto, L., *J. Chem. Phys*. **80**, 4441 (1984). (e) Enciso, E., Lado, F., Lombardero, M., Abascal, J.L.F. and Lago, S., *J. Chem. Phys*. **87**, 2249 (1987). Note that the bridge function in these and related papers is sometimes defined, in the present notation, as $-b(r)$.
[36] See Note 14. The hard-sphere bridge function has also been parameterised as a function of packing fraction by Malijevský, A. and Labík, S., *Mol. Phys*. **60**, 663 (1987).
[37] See, e.g. Kambayashi, S. and Chihara, J., *Phys. Rev. E* **50**, 1317 (1994).
[38] Rogers, F.J. and Young, D.A., *Phys. Rev. A* **30**, 999 (1984).
[39] Zerah, G. and Hansen, J.P., *J. Chem. Phys*. **84**, 2336 (1986).
[40] (a) Pini, D., Stell, G. and Høye, J.S., *Int. J. Thermophys*. **19**, 1029 (1998). (b) Pini, D., Stell, G. and Wilding, N.B., *Mol. Phys*. **95**, 483 (1998). (c) Caccamo, C., Pellicane, G., Costa, D., Pini, D. and Stell, G., *Phys. Rev. E* **60**, 5533 (1999). (d) Kahl, G., Schöll-Paschinger, E. and Stell, G., *J. Phys. Condensed Matter* **14**, 9153 (2002).
[41] This result follows straightforwardly from the thermodynamic relations (2.3.8) and (2.3.9).
[42] (a) Waisman, E., *Mol. Phys*. **25**, 45 (1973). (b) For later developments see, e.g. Høye, J.S. and Blum, L., *J. Stat. Phys*. **16**, 399 (1977). (c) Ginoza, M., *Mol. Phys*. **71**, 145 (1990). (d) Tang, Y., *J. Chem. Phys*. **118**, 4140 (2003).
[43] See, e.g. Pini, D., Stell, G. and Wilding, N.B., *J. Chem. Phys*. **115**, 2702 (2001).
[44] (a) Schöll-Paschinger, E., Benavides, A.L. and Castañeda-Priego, R., *J. Chem. Phys*. **123**, 234513 (2005). (b) Pini, D., Parola, A., Colombo, J. and Reatto, L., *Mol. Phys*. **109**, 1343 (2011).
[45] (a) Del Río, F., Avalos, E., Espíndola, R., Rull, L.F., Jackson, G. and Lago, S., *Mol. Phys*. **100**, 2531 (2002) (closed circles). (b) Largo, J., Miller, M.A. and Sciortino, F., *J. Chem. Phys*. **128**, 134513 (2008) (open circles).
[46] Orea, P., Tapia-Medina, C., Pini, D. and Reiner, A., *J. Chem. Phys*. **132**, 114108 (2010).
[47] Fisher, M.E. and Widom, B., *J. Chem. Phys*. **50**, 3756 (1969).
[48] (a) Evans, R., Leote de Carvalho, R.J.F., Henderson, J.R. and Hoyle, D.C., *J. Chem. Phys*. **100**, 591 (1994). (b) Leote de Carvalho, R.J.F., Evans, R., Hoyle, D.C. and Henderson, J.R., *J. Phys. Condensed Matter* **6**, 9275 (1994). In these papers the notation $\alpha_1 \equiv k_1$, $\alpha_0 \equiv k_2$ is used.
[49] The potential is also shifted upwards to make it vanish at the truncation distance.
[50] Smit, B., *J. Chem. Phys*. **96**, 8639 (1992).
[51] Enderby, J.E., Gaskell, T. and March, N.H., *Proc. Phys. Soc*. **85**, 217 (1965).
[52] Evans, R. and Henderson, J.R., *J. Phys.: Condensed Matter* **21**, 474220 (2009).
[53] Leote de Carvalho, R.J.F. and Evans, R., *Mol. Phys*. **83**, 619 (1994).